Barrier Effect of the Indo-Pacific Maritime Continent on the MJO: Perspectives from Tracking MJO Precipitation

CHIDONG ZHANG

NOAA/Pacific Marine Environmental Laboratory, Seattle, Washington

JIAN LING

State Key Laboratory of Numerical Modeling for Atmospheric Sciences and Geophysical Fluid Dynamics, Institute of Atmospheric Physics, Chinese Academy of Sciences, and University of Chinese Academy of Sciences, Beijing, China

(Manuscript received 18 August 2016, in final form 12 January 2017)

ABSTRACT

Explanations for the barrier effect of the Indo-Pacific Maritime Continent (MC) on the MJO should satisfy two criteria. First, they should include specific features of the MC, namely, its intricate land–sea distributions and elevated terrains. Second, they should include mechanisms for both the barrier effect and its overcoming by some MJO events. Guided by these two criteria, a precipitation-tracking method is applied to identify MJO events that propagate across the MC (MJO-C) and those that are blocked by the MC (MJO-B). About a half of MJO events that form over the Indian Ocean propagate through the MC. Most of them (>75%) become weakened over the MC. The barrier effect cannot be explained in terms of the strength, horizontal scale, or spatial distribution of MJO convection when it approaches the MC from the west. A distinction between MJO-B and MJO-C is their precipitation over the sea versus land in the MC region. MJO-C events rain much more over the sea than over land, whereas rainfall over the sea never becomes dominant for MJO-B. This suggests that inhibiting convective development over the sea could be a possible mechanism for the barrier effect of the MC. Preceding conditions for MJO-C include stronger low-level zonal moisture flux convergence and higher SST in the MC region. Possible connections between these large-scale conditions and the land versus sea distributions of MJO rainfall through the diurnal cycle are discussed.

1. Introduction

The Madden–Julian oscillation (MJO; Madden and Julian 1971, 1972) is a primary source of predictability of the Earth system on subseasonal (3–6 weeks) time scales (Waliser et al. 2003). As the MJO moves eastward, its influences on many environmental hazards (e.g., tropical cyclones, cold surges, heat waves, lightning, and flood) and climate modes [e.g., Indian Ocean dipole (IOD), ENSO, and NAO] depend on whether its convection center is over the Indian Ocean, the Indo-Pacific Maritime Continent (MC), or the Pacific (Zhang 2013). Teleconnection patterns from the tropics to extratropics generated by the MJO are the strongest when its convection center is located near the eastern edge of the MC (Adames and Wallace 2014). An example of MJO remote influences is the record warm temperatures over the United States in March 2012 that have been attributed to an active MJO event propagating through the MC (Dole et al. 2014).

The behavior of the MJO over the MC is very different from that over the open water of the Indian and Pacific Oceans. In observations, when the MJO propagates over the MC, it often weakens, its propagation speed becomes uneven, and it may completely break down and fail to reemerge on the Pacific side (Rui and Wang 1990; Hendon and Salby 1994; Hsu and Lee 2005; Kim et al. 2014). The weakening and blocking of the MJO by the MC is known as a "barrier effect" on MJO propagation. This barrier effect of the MC in nature is often exaggerated in numerical models (Inness and Slingo 2003; Kim et al. 2009; Seo et al. 2009), creating an MJO "prediction barrier" (Weaver et al. 2011; Fu et al. 2013). For example, the fraction of MJO events that fail to propagate through

Pacific Marine Environmental Laboratory Contribution Number 4598.

Corresponding author e-mail: Jian Ling, lingjian@lasg.iap.ac.cn

DOI: 10.1175/JCLI-D-16-0614.1

© 2017 American Meteorological Society. For information regarding reuse of this content and general copyright information, consult the AMS Copyright Policy (www.ametsoc.org/PUBSReuseLicenses).

Unauthenticated | Downloaded 12/28/22 07:27 PM UTC

the MC is 30% in a global reanalysis product but 50% in the ECMWF forecast system (Vitart and Molteni 2010). The MJO prediction barrier would inevitably undermine the model capability of forecasting global influences of the MJO (Hendon et al. 2000) and hinder the overall model capability of subseasonal prediction.

Several possible reasons for the MC barrier effect on MJO propagation have been suggested. If surface fluxes, especially latent heat flux, are important to the MJO (Maloney and Sobel 2004; Sobel et al. 2008), then the MJO would be weakened or diminished by the reduction in surface fluxes in the MC region because of its many islands. If moisture convergence of the low-level circulation is essential to the MJO (Wang 1988; 2005), then its distortion by topographic interference would impair the MJO (Hsu and Lee 2005; Inness and Slingo 2006; Wu and Hsu 2009). It has been suggested that cloud–radiation interaction is the source of instability for the MJO and sets its intraseasonal rhythm (Hu and Randall 1994, 1995; Sobel and Maloney 2013; Adames and Kim 2016). This interaction can be interrupted by persistent diurnal convection over islands (Neale and Slingo 2003; Hagos et al. 2016) that is almost synchronized throughout the MC. The diurnal cycle in the MC may make it difficult for the MJO to propagate through its rectified influences on the symmetric and asymmetric components of the MJO (Tung et al. 2014; Majda and Yang 2016). It has been suggested that the barrier effect mainly comes from large-scale circulations that modulate moisture distributions downstream over the western Pacific (Kim et al. 2014; Feng et al. 2015). A strong initial wet bias in rainfall and a cold bias in sea surface temperature over or near the MC are found unfavorable for MJO to propagate through in ensemble predictions of the ECMWF (Kim et al. 2016). While all these factors are plausible, satisfactory explanations for the MC barrier effect on the MJO in nature and its exaggeration in numerical models are still missing for the reasons discussed below.

In this study, we intend to contribute to the current effort of understanding the barrier effect of the MC on the MJO. While finding a definite explanation for the barrier effect in a single study is a tall expectation, we strive to explore possible processes that have not been thoroughly investigated by previous studies. At the very least, we attempt to unravel aspects of the barrier effect that may serve as targets for more focused studies in the future. For the ease of discussion, we will refer to MJO events that are successful in crossing the MC as MJO crossing (MJO-C) and those that are blocked by the MC as MJO blocked (MJO-B). Before we describe the design of our study and its results, we wish to introduce our thoughts on the issue of the barrier effect, which have served to guide this study.

An acceptable explanation for the barrier effect of the MC should satisfy at least two criteria. First, it should include the specific features of the MC that distinguish it from the open oceans of the Indo-Pacific region where the MJO thrives. These features are the intricate land–sea distribution and elevated terrains. The possible explanations of the barrier effect in terms of blocking of surface fluxes by land, topographic interference of the low-level circulation, and the diurnal cycle of land convection discussed earlier all meet this criterion. The explanations in terms of the large-scale circulation over the western Pacific are connected to the MC only implicitly through the dependence of the mean state on the MC. Without this dependence, the large-scale circulation may "accidentally" make the MJO weakened and diminished more often over the MC than anywhere else, and the barrier effect may exist not because of the MC.

The second criterion is that they should elucidate not only why MJO-B events fail to propagate through the MC, but also why such a barrier effect can be overcome by MJO-C events. Because the islands are present in the MC for all MJO events, there are only two possibilities that may distinguish MJO-C from MJO-B. One is a large-scale condition that is independent of the MJO. The other is the MJO itself. Intuitively, strong MJO events would have a greater chance than weak ones to survive the barrier effect of the MC. This, however, has never been quantitatively demonstrated. It is possible that overcoming the barrier effect depends on both the MJO itself and its large-scale conditions. None of the existing explanations of the MC barrier effect meets this second criterion as well as the first one.

Guided by these thoughts, we investigated in this study the barrier effect of the MC on the MJO with two unique aspects that distinguish ours from previous studies on the same subject. The first is a method of tracking MJO precipitation, which has been used by Ling et al. (2014) to compare global versus local MJO prediction skills. Using this method, we identified MJO events, separated MJO-B from MJO-C, and obtained quantitative information of the barrier effect that was unavailable before. The second distinct aspect of this study is that we examined detailed distributions of the MJO precipitation over the sea and land in the MC for MJO-B and MJO-C, as well as their large-scale conditions.

In the rest of this article, we describe the data used in section 2 and the procedures of identifying eastward-propagating precipitation events in section 3 and identifying MJO events in section 4. We introduce in section 5 basic statistics of tracked MJO events and quantitative information of the barrier effect. In section 6, we present comparisons of MJO-B and MJO-C, including their large-scale features in precipitation (section 6a), detailed distributions of precipitation over the sea and land in the MC region (section 6b), and large-scale conditions

Unauthenticated | Downloaded 12/28/22 07:27 PM UTC

over the MC (section 6c). A summary, further discussions, and concluding remarks are given in section 7.

2. Data

The following data were used in this study:

1) Daily rainfall (0.25° × 0.25°) from Tropical Rainfall Measuring Mission (TRMM) 3B42 version 7 (3B42v7) Multisatellite Precipitation Analysis (Huffman et al. 2007) that covers the period of 1998–2015 was used to develop the tracking method (section 3), following Ling et al. (2014).
2) Pentad mean CPC Merged Analysis of Precipitation (CMAP) rainfall (Xie and Arkin 1997), available for 1979–2014, was used because its longer period provides more samples of the MJO than the TRMM data for robust statistics. For direct comparisons, the CMAP data were interpolated from their original pentad and 2.5° × 2.5° grids to the TRMM daily and 0.25° × 0.25° grids.
3) Daily mean TRMM Microwave Imager (TMI) SST version 7.1 (Gentemann et al. 2010) dataset is more suitable to describing SST in the MC region than other SST data because of its relatively high horizontal resolution (0.25° × 0.25°) and the capability of TMI to penetrate through clouds. This dataset covers the period of 1998–2014.
4) All-season Real-Time Multivariate MJO (RMM) index of Wheeler and Hendon (2004) is commonly used in MJO studies, including those on the barrier effect of the MC. It was used in this study to compare with results derived from the method of tracking MJO precipitation.
5) Daily zonal, meridional, and vertical wind and specific humidity from the ECMWF interim reanalysis (ERA-Interim, hereafter ERA-I; Dee et al. 2011) were used to calculate the larger-scale circulation and moisture flux convergence. The horizontal resolution of this dataset is 0.75° × 0.75°. Its vertical resolutions are 25 hPa between 1000 and 750 hPa, 50 hPa between 750 and 250 hPa, and 25 hPa between 250 and 100 hPa.
6) Surface (10 m) winds from QuikSCAT (Spencer et al. 2000; Hoffman and Leidner 2005) covering 1999–2009 and WindSat (Gaiser et al. 2004) covering 2010–15 were used to supplement the ERA-I data. These two datasets have a horizontal resolution of 0.25° × 0.25° and, in combination, cover the period of TRMM.

3. Tracking of eastward-moving precipitation

The MJO tracking method used in this study is an updated version of the one introduced by Ling et al. (2014). Its basic idea is to objectively identify the eastward movement of positive precipitation anomalies along the equator with certain characteristics consistent to the known canonical MJO. With a priori criteria that have to be defined subjectively, this method allows individual MJO events to be identified without further human intervention, hence objectively. Also provided by the method are several variables of the identified MJO events, such as their starting and ending longitudes and time, propagation speeds and ranges (in longitude), strength (in terms of precipitation), life spans, zonal scales (in longitude), and intervals between two adjacent events. All these quantities are not available from EOF-based MJO indices (Wheeler and Hendon 2004; Kiladis et al. 2014; Lafleur et al. 2015; Liu et al. 2016).

This tracking method consists of three main procedures: data preparation, tracking eastward movement of positive anomalies in precipitation, and selecting MJO events. The method is described below with sufficient details for independent reproduction of our results.

The data preparation started with calculating daily anomalies in precipitation by removing daily climatology (omitting 29 February in leap years). A two-dimensional fast Fourier transform was used to obtain the large-scale (zonal wavenumbers 1–10) eastward-propagating intraseasonal (20–100 day) signals (Gottschalck et al. 2013). The filtered precipitation anomalies were then averaged over a latitude belt of 15°S–15°N, which is considered as the tropics based on the zonal and time mean distribution of potential vorticity (Zhang and Ling 2012). In this article, the equatorial anomalies in precipitation will be denoted as $P'(x, t)$, or simply P'. Standard deviations of P' were calculated at each longitude grid point, which will be denoted as $\sigma_P(x)$, or simply σ_P.

Tracking of eastward movement of positive anomalies in precipitation was done using P' with the following steps (see Fig. 1):

(i) Select a reference longitude x_0 and a tracking domain. The reference longitude in this study is 90°E for effectively identifying MJO events over the Indian Ocean. The tracking domain is eastward from 40°W to 120°W. This broad domain was used to capture the MJO in both the Indian and Pacific Oceans.
(ii) Run a set of straight lines passing the reference longitude at a given day t_0, each with its own slope (solid thin blue lines in Fig. 1a). They are trial (tracking) lines. The slope of each trial line represents the zonal propagation direction and speed. With choices of the line slopes, this method can be

Unauthenticated | Downloaded 12/28/22 07:27 PM UTC

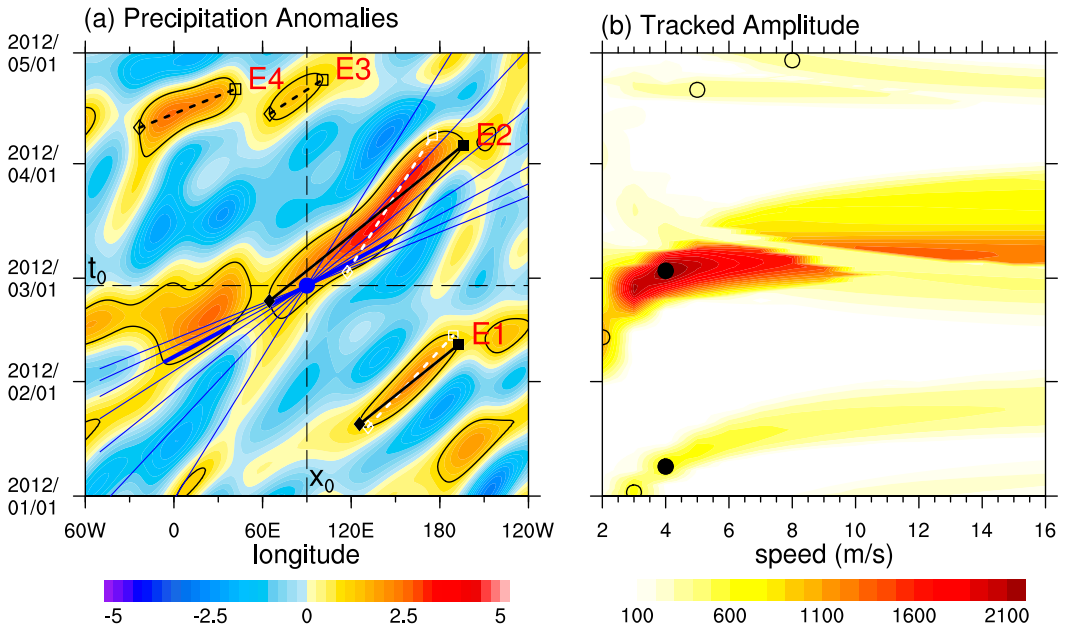

FIG. 1. Illustration of the tracking method applied to 1 Jan–1 May 2012. (a) Time–longitude diagram of anomalous precipitation (mm day^{-1}). Precipitation envelopes (areas of $P' > \sigma_P$) are enclosed by black contours; x_0 and t_0 are reference longitude and time, respectively. Thin blue lines are trial tracking lines. Thick blue lines are examples of segments with $P' > \sigma_P$ along a trial tracking line. Black dashed lines are eliminated segments. White dashed lines are segments not selected for the MJO. Thick black lines are the final selected MJO tracks. (b) Tracked amplitudes (kg m^{-1} s^{-1}) as functions of the speed (slope of tracking lines) and the time when a trial line crosses the reference longitude x_0. Black dots marks $A_m(t, s)$ for events E1 and E2 in (a), based on which of the final tracks [thick black lines in (a)] of the MJO event are selected. Open circles represent local maximum amplitudes $A_m(t, s)$ corresponding to unselected segments (for events E1 and E2) and unselected events (E3 and E4). See text for more details.

equally applied to track eastward- and westward-propagating P'. In this study, only eastward-propagating P' was tracked.

(iii) Identify a longest segment along each trial line that satisfied $P' > \sigma_P$ continuously (e.g., the longer solid thick blue line in Fig. 1a). If a gap between two neighboring segments of $P' > \sigma_P$ is smaller than 10° longitude, then they are considered joined and treated as one segment.

(iv) Calculate the amplitude of each selected segment as integrated P' along the segment $A(t_0, s)$ where s represents the slope of the trial line (or speed of the event) passing through the reference longitude at day t_0.

(v) Repeat steps (ii)–(iv) for each day. As a result, amplitudes of all selected segments are expressed as a two-dimensional function $A(t, s)$ for all days (Fig. 1b).

(vi) Identify eastward-propagating precipitation events. Local maxima in A, denoted as $A_m(t, s)$, are identified as peaks centered on an 11-day running window. Their examples are marked by dots and open circles in Fig. 1b. Each $A_m(t, s)$ represents a selected segment along a trial line that crosses the reference longitude at time t with a propagation speed s. If there are two segments within the same eastward-moving precipitation envelop (areas of $P' > \sigma_P$ enclosed by black contours in Fig. 1a), the one with the greater amplitude is retained and the other neglected (e.g., dashed white lines of events E1 and E2 in Fig. 1a are discarded for their smaller amplitudes). The remaining selected segments will be referred to as tracks for eastward-propagating events (thick solid and dashed black lines in Fig. 1a).

Once eastward-moving precipitation events are identified, their several characteristics (illustrated in Fig. 2) can be quantified in addition to the speed and amplitude. A starting point (black diamonds in Fig. 2) and ending point (black squares) correspond to the starting and ending longitudes and dates of a track, respectively. Averaged strength is the rain rate averaged along a track from its starting to ending points. A propagation range is the distance of a track between its starting and ending longitudes. A life span is the time between the starting and ending dates of a track. A daily zonal scale is the zonal coverage of a precipitation envelope $P' > \sigma_P$ for a track at a given day, and a mean zonal scale of an event is the average of its daily zonal scales through its entire life span. An interval is the time between the starting dates of two adjacent events.

There are a total of 190 eastward-moving precipitation events identified using the TRMM data. All

Unauthenticated | Downloaded 12/28/22 07:27 PM UTC

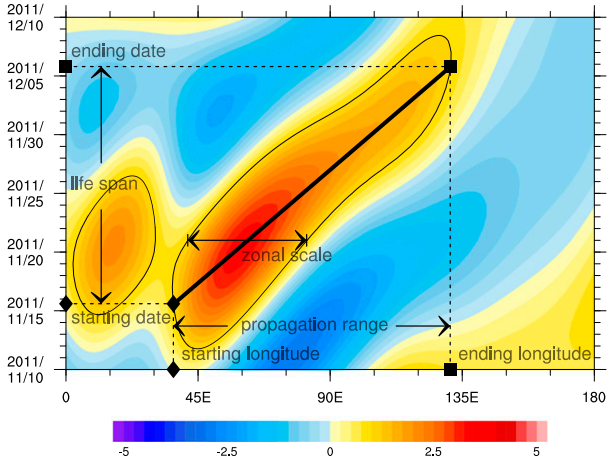

FIG. 2. As in Fig. 1a, but for definitions of quantities of eastward-moving precipitation events. The thick black line is an MJO track. Thin black contours encircle areas of $P' > \sigma_P$, which are precipitation (or convection) envelopes. See text for other details.

are not the MJO. For example, while the eastward-moving speed of most tracked events is 3–7 m s^{-1}, a few have slower or faster speeds (Fig. 3a). Most tracked events propagate over a distance greater than 50° longitude, but some propagate over a distance shorter than that (Fig. 3b). The interval between two adjacent tracked events range from 10 to 80 days (Fig. 3c). The mean zonal scale of tracked events can be as small as 10° and as large as 75° longitude (Fig. 3d).

These statistical distributions of tracked eastward-moving events in precipitation illustrate a continuum nature of the MJO: There is a broad range of eastward-moving events in precipitation. The canonical MJO as we know from composites based on EOF analysis (e.g., the RMM index) is embedded within the group of these eastward-moving events. There is, however, no clear distinction between the canonical MJO and other "non-MJO" eastward propagation events by any definition. Roundy (2012) pointed out the continuum nature of the MJO and convectively coupled Kelvin waves. This continuum nature exists for all large-scale eastward-propagating precipitation events, as demonstrated in Fig. 3. The broad range of eastward-propagating precipitation events is not a unique result of our tracking method. It emerges also from other methods designed for detecting the MJO. For example, when the RMM index (Wheeler and Hendon 2004) is used to identify individual MJO events based on a single criterion of amplitude greater than one standard deviation, also included are many other events that are not consistent to the known canonical MJO but not distinctively separated from the canonical MJO (Roundy et al. 2009; Straub 2013).

Apparently, additional criteria are needed to select the MJO from all tracked eastward-moving events. These criteria cannot be determined in a completely objective way. They depend on one's perception of the MJO, objective, and, perhaps, convenience. Determining these criteria does not fundamentally differ from determining the width of bandpass filtering that is commonly used in MJO studies. There is always an issue of how sensitive the final results might be to the choices of the criteria. But once these criteria are determined, the results should be reproducible.

4. Selection of MJO events

MJO events were selected from all tracked eastward-moving precipitation events based on the following criteria:

1) The propagation range is greater than 50° longitude. This criterion is designed to select MJO events that propagate over at least a distance equivalent to the width of the tropical Indian Ocean. For example, eastward-moving event E3 in Fig. 1a does not meet this criterion and is not considered an MJO event. This criterion alone would eliminate 30% (56 out of 190) of all tracked events.
2) Propagation speed is between 3 and 7 m s^{-1}. An example is eastward-moving event E4 in Fig. 1a, which was eliminated because its speed is 8 m s^{-1}. There is no physical justification for this particular range of speed for the MJO versus a wider or narrower one. The main reason for this choice is to exclude outliers. Most fast events are not only inconsistent to the known canonical MJO, but also weaker and shorter lived than slow events. Totally 17% (33 out of 190) of all tracked events would be eliminated by this criterion alone.
3) The interval is greater than 20 days. This is to ensure the intraseasonal time scale of the MJO. Aliasing of the 20–100-day bandpass filtering (section 3) permits tracked events to occur within 20 days from each other. If there is more than one event initiated within a 20-day running window, only the one with the greatest amplitude is retained. This criterion alone would eliminate 25% (47 out of 190) of all tracked events.

Eastward-moving events in precipitation anomalies P' satisfying all these criteria 1–3 are considered MJO events. The segments of $P' > \sigma_P$ along selected tracking lines representing the MJO events are referred to herein as MJO tracks (thick solid black lines in Fig. 1a). There are a total of 100 MJO events identified using the TRMM data, 52.6% of all tracked events.

Unauthenticated | Downloaded 12/28/22 07:27 PM UTC

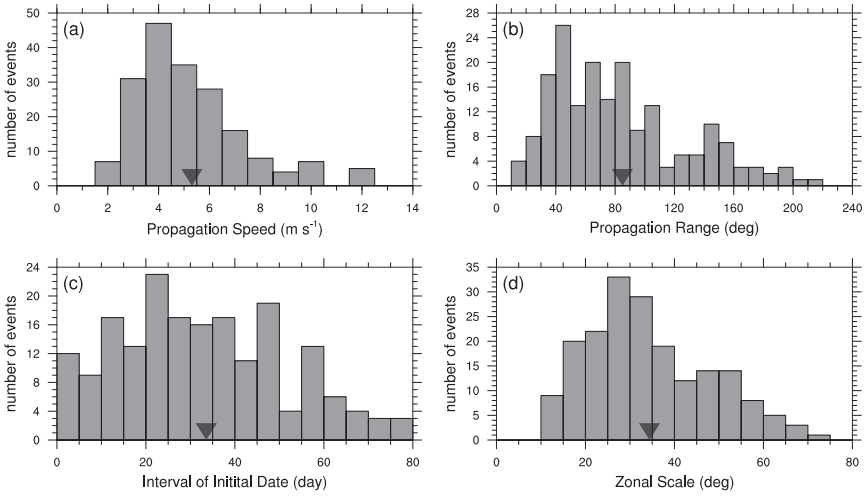

FIG. 3. Number distributions by (a) speeds, (b) propagation ranges, (c) intervals, and (d) averaged zonal scales of all tracked eastward-moving events based on the TRMM precipitation data. Their means are marked by triangles.

This tracking method yields quantitative information about the MJO (e.g., starting and ending dates and longitudes, life span, zonal scale, propagation speed and range, and exact longitudinal location of MJO convection center) that is not all available from MJO indices based on global EOF analysis (Wheeler and Hendon 2004; Kiladis et al. 2014; Liu et al. 2016). This is one of the major advantages of this MJO tracking method. Its main weakness is that several criteria need to be determined subjectively. Consistent results were nevertheless obtained when some of the subjectively chosen criteria were removed or changed slightly. For example, not allowing neighboring segments of $P' > \sigma_P$ with their gaps $<10°$ to joint together modifies the total number of the tracked eastward-moving precipitation events and identified MJO events by less than 5%. This does not change the final results. We kept this procedure because it makes physical sense: An MJO event may temporarily become weak and bounce back again. We also tested the sensitivity of our results to the criteria used to select MJO events by expanding the longitudinal range from 50° to 60°, the speed range from 3–7 to 3–8 m s^{-1}, and the interval from 20 to 25 days. As a consequence, the total number of tracked MJO events varies from 92 to 105. Results reported in the rest of this article remain qualitatively the same. Our results depend on neither the choice of the reference longitude as long as it is in the central Indian Ocean nor the range of tracking as long as it covers the Indo-Pacific warm pool. These sensitivity tests lend us confidence that our results are robust and reproducible.

Kerns and Chen (2016) developed a different method of tracking MJO precipitation. Their method defines large-scale precipitation envelopes and follows their movement. Their method tracks two-dimensional motions of MJO precipitation in longitude and latitude; ours tracks one-dimensional motions in longitude. While latitudinal positions of convection centers of the MJO are important for overcoming the barrier effect of the MC (see section 6a), we in this study primarily focus on the first-order feature of the MJO: its zonal propagation. Three-dimensional structures and evolution of the MJO and its environment can be reconstructed once individual MJO events are identified. This will be illustrated later in this article.

5. Statistics of the tracked MJO and barrier effect

Some quantities of the MJO derived from the tracking method can be compared with that derived using different methods (Lafleur et al. 2015); others are previously unavailable. The distribution of starting longitudes indicates that MJO events may form almost anywhere in the tropics, as suggested by Matthews (2008), but most of them form over the Indian Ocean (the ordinate in Fig. 4a). The distribution of ending longitudes exhibits two peaks: one over the MC and the other over the central Pacific (the abscissa in Fig. 4a). This is direct evidence for the MC barrier effect on the MJO: an MJO event either fails to propagate through the MC and vanishes there or, if it survives the MC, continues to move eastward until it reaches the cold sea surface east of the western Pacific warm pool. There is no other explanation for the two peaks. These two peaks rule out any explanation for the barrier effect in terms of

Unauthenticated | Downloaded 12/28/22 07:27 PM UTC

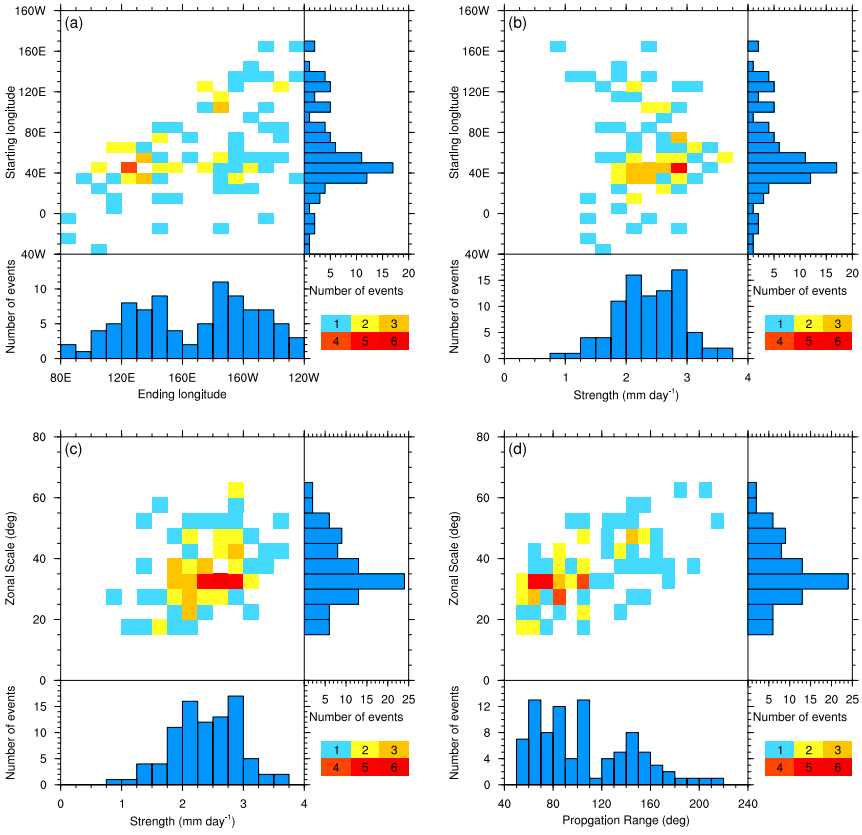

FIG. 4. Individual and joint number distributions of (a) starting vs ending longitudes, (b) starting longitudes vs mean strength, (c) mean zonal scales vs mean strength, and (d) mean zonal scales vs propagation ranges of tracked MJO events using the TRMM precipitation data. Colors of the joint distributions represent the number of events.

large-scale circulation patterns that are not direct consequences of the MC.

Few MJO events that form over the Atlantic Ocean (starting longitudes <40°E) and over the western Pacific (starting longitudes >150°E) are all relatively weak compared to the rest (Fig. 4b). In general, there is no clear connection between the mean strength and zonal scale of the MJO, except the weakest are all small (Fig. 4c). There is, however, a clear relationship between their zonal scales and propagation ranges: MJO events of larger zonal scales tend to propagate over longer distances (Fig. 4d). The two peaks in propagation ranges correspond well to the two peaks in the ending longitudes: Most MJO events with short ranges form over the Indian Ocean and terminate over the MC; most with long ranges propagate through the MC and terminate over the central Pacific. These results suggest that MJO events with larger zonal scales should have a greater chance to propagate through the MC. This is true only to a limited extent. Few extremely large MJO events (zonal scales >55° longitude) all propagate through the MC, while some MJO events with small zonal scales (<30° longitude) also do (not shown).

To increase our sample sizes for tracked MJO events, we applied the tracking method to the CMAP data, which cover a longer period (1979–2014) than the TRMM data (1998–2015).[1] The total number of tracked MJO events using CMAP is 172. In the following, we compare results from TRMM and CMAP in the context of the MC barrier effect on the MJO to seek robust results that are independent of data used.

There are two manifestations of the barrier effect of the MC on the MJO. One is blocking MJO propagation, as suggested by the two peaks in the distribution of ending longitudes of tracked MJO events in Fig. 4a. This figure is reproduced in Fig. 5a for tracked MJO events that start over the Indian Ocean (e.g., on their starting dates, areas of precipitation anomalies $P' > \sigma_P$ are

[1] We also tried to use OLR but influences from high, thick cirrus are problematic for tracking the motion of MJO convection.

Unauthenticated | Downloaded 12/28/22 07:27 PM UTC

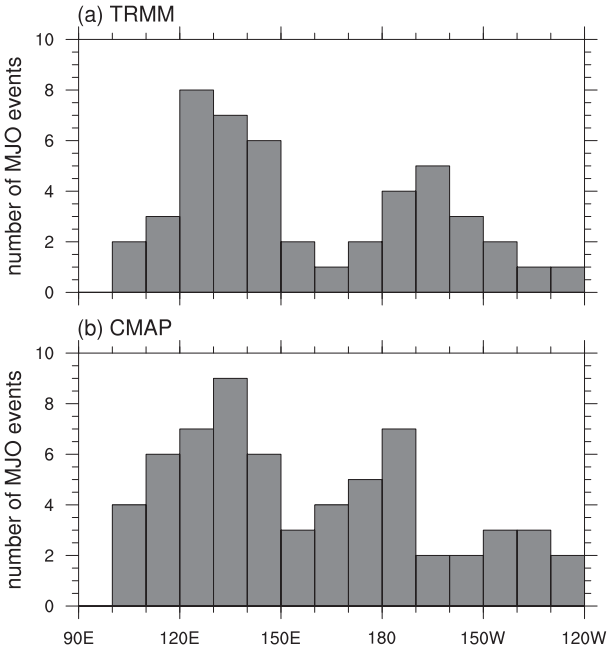

FIG. 5. Zonal distributions of ending longitudes of tracked MJO events that start over the Indian Ocean based on the (a) TRMM and (b) CMAP data.

between 30° and 100°E). The two peaks in Figs. 4a and 5a suggest two distinct groups of the MJO: MJO-C events that are successful in crossing the MC (with their ending longitudes east of 150°E) and MJO-B events that are blocked by the MC (with their ending longitudes over the MC: i.e., 100°–150°E). We wish to point out that the term ''nonpropagating MJO events,'' used in other studies (Kim et al. 2014; Feng et al. 2015), is not appropriate for MJO-B events defined here, which propagate eastward by definition but not through the MC. The second barrier effect is the weakening of MJO events over the MC regardless of whether they propagate through. This effect is demonstrated in Figs. 6a and 6b, where strength of each MJO event formed over the Indian Ocean is plotted as a function of longitude along its track.

These two MC barrier effects on the MJO based on the TRMM data are well reproduced from the CMAP data. The distributions of ending longitudes of tracked MJO events based on the two datasets show detailed differences, but the two peaks over the MC and central Pacific, respectively, are present in both (Fig. 5b). The weakening of MJO events over the MC seen in the TRMM data is also reproduced from the CMAP data (Figs. 6c,d). Based on the TRMM data, out of all MJO-C events, 75% (18 out of 24) are weakened over the MC, measured by the ratio of the averaged strength along their tracks within 120°–130°E to that of 90°–100°E; 82% (27 out of 33) are weakened based on the CMAP data.

Of all tracked MJO events that start over the Indian Ocean, 50% (12 out of 24) are MJO-B in boreal winter and 54% (14 out of 26) in boreal summer based on the TRMM data; based on the CMAP data, 42% (15 out of 36) and 59% (17 out of 29) are in boreal winter and summer, respectively. In comparison, Kerns and Chen (2016) reported that 43% of MJO events identified by their large-scale precipitation tracking are MJO-B. Based on these consistent results, about half of MJO events formed over the Indian Ocean fail to propagate through the MC.

These percentages of MJO-B events identified by tracking precipitation of the MJO are much larger than that (30%) found by Vitart and Molteni (2010) based on the RMM index of Wheeler and Hendon (2004). A more detailed comparison between the results based on the two methods is warranted. The distinctions between MJO-B and MJO-C identified by our tracking method are clearly captured by the RMM index (Fig. 7). The averaged RMM amplitude is almost always smaller than 1 for MJO-B (blue curve), whereas it is larger than 1 for MJO-C (red) over the Indian Ocean (phases 2 and 3), the MC (phases 4 and 5), and the western Pacific (phases 6 and 7). The barrier effect of weakening is clearly demonstrated by the reduction in amplitude of the averaged RMM amplitude for MJO-C (red) over the MC (phases 4 and 5). The barrier effect of blocking is seen as the mean amplitude of MJO-B (blue) quickly approaches zero over the western Pacific (phase 6). These are consistent with the results based on our MJO tracking method.

There are discrepancies between the descriptions of the barrier effect by the RMM index and MJO tracking that require careful interpretations. The RMM index suggests MJO-C is much stronger than MJO-B before they enter the MC (phase 3). This is not the case in precipitation, as we will discuss in section 6a. Mean MJO-B is hardly recognized by the RMM index as the MJO because its amplitude is smaller than one most of the time. These differences come mainly from the fact that the RMM index represents the zonal wind component of the MJO more than its convection component (Straub 2013). The stronger circulation of MJO-C than MJO-B can indeed be seen from its composites (section 6a). Many MJO-B events are not recognized by the RMM index based on the criterion of amplitude greater than one because their propagation ranges are small, their life spans are short, and thus they do not generate strong global responses in the zonal wind. This explains the relatively small percentage of MJO-B based on the RMM index found by Vitart and Molteni (2010). The

Unauthenticated | Downloaded 12/28/22 07:27 PM UTC

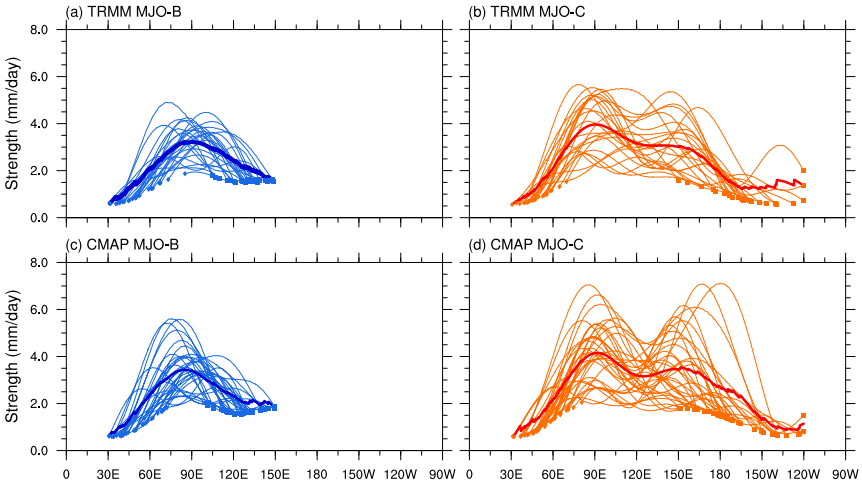

FIG. 6. Strength (mm day^{-1}) as a function of longitude along the track ($P' > \sigma_P$) for each MJO event that starts over the Indian Ocean for (a) MJO-B and (b) MJO-C based on the TRMM precipitation data and (c) MJO-B and (d) MJO-C based on the CMAP data. Thick lines are their respective means. Starting points of the tracks are marked by diamonds and ending points by squares.

inability of the RMM index to accurately represent the location of convection center of the MJO is also illustrated in Fig. 7. Longitudes of convective centers for MJO-B and MJO-C identified by our tracking method (e.g., 80°, 120°, and 140°E) may end up in different RMM phases.

Most (83%) successive MJO events (Matthews 2008), which follow a previous MJO event within 60 days, are MJO-B. The primary MJO without a previous event within 60 days includes slightly more (60%) MJO-C. This suggests that an MJO event tends to be followed by another one, but the barrier effect of the MC is a major mechanism that terminates a series of successive MJO events.

6. Comparisons between MJO-B and MJO-C

In this section, we further compare MJO-B and MJO-C to seek differences that may provide insights to physical mechanisms for the barrier effect of the MC and its overcoming. We used CMAP for its longer record for large-scale features and TRMM precipitation with its higher resolution for more detailed spatial distributions within the MC region.

For a composite of a given field, the Student's t test was used to assess its significance at the 95% confidence level. For assessing the significance of wind vectors, the Student's t test was applied to each of its components. A composite of wind vector is considered significant if either one component passes the test. The degree of freedom was estimated using the number of events that went into the composite. When comparing a given field over a certain area between MJO-B and MJO-C, we started with a null hypothesis that its probability distribution functions (PDFs) for the two are from the same population (i.e., nondistinguishable). This field would be significantly different for the two types of the MJO if this null hypothesis is rejected by the Kolmogorov–Smirnov (KS) test at the 95% confidence level. In the rest of this article, the term "significant" is used to indicate the 95% confidence level in either the Student's t or KS test.

Propagation speeds for individual MJO events span from 3 to 7 m s^{-1}. This may lead to distortions in time-lag composites using fixed time intervals relative to the reference point (day 0). To avoid this, we made averages over days when MJO tracks (or its extension) pass a given longitude (equivalent to their convection centers located at a given longitude) unless otherwise mentioned.

a. Large-scale MJO precipitation

The barrier effect of weakening the MJO over the MC is further demonstrated in Fig. 8. This figure shows the distribution of the ratio of MJO strength $A(x)/A(x_0)$, where x represents longitudinal bins of 5° from 100°E to 180°, x_0 represents a fixed longitude bin of 90°–100°E, and A is CMAP P' averaged within a longitudinal bin along each MJO track. This figure shows how amplitudes of MJO events vary after they enter the MC. Most MJO events become weaker immediately after their tracks pass 100°E. The main difference is MJO-C events manage to recover their strength over the eastern MC (Fig. 8b), while MJO-B events do not (Fig. 8a).

Unauthenticated | Downloaded 12/28/22 07:27 PM UTC

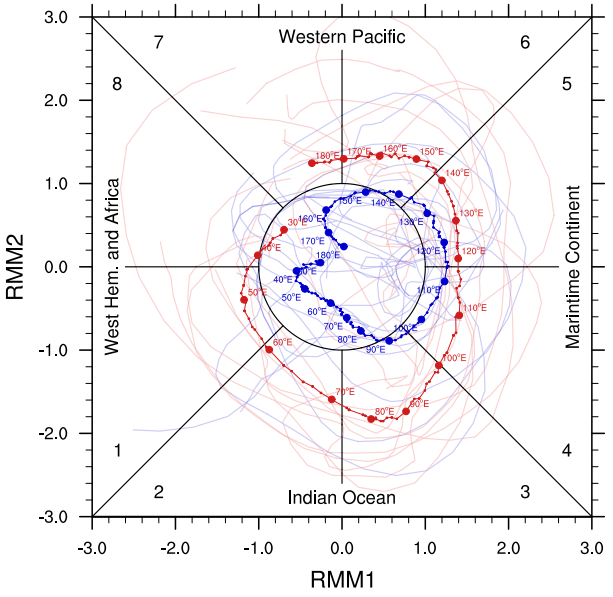

FIG. 7. RMM index for MJO-B (blue) and MJO-C (red) identified using the CMAP data. Thin lines are for individual events. Thick lines are averages of the amplitudes of individual tracks over each 1° longitude. Selected longitudes of the mean tracks are marked.

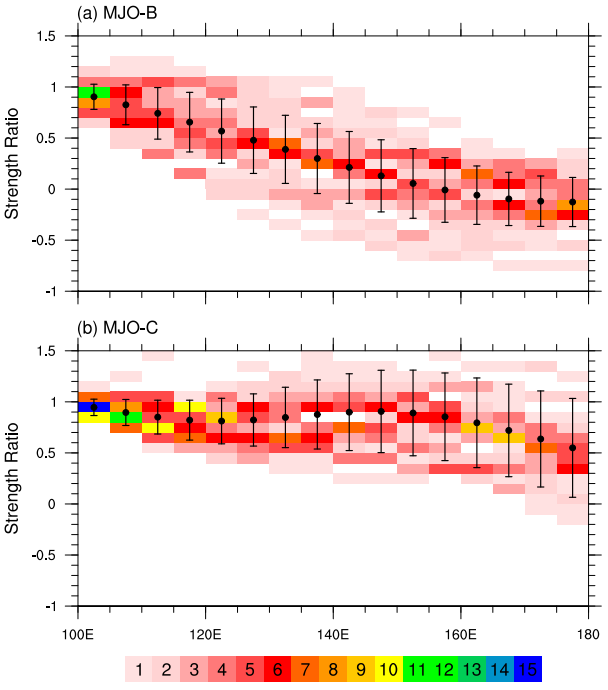

FIG. 8. Ratio of MJO strength $A(x)/A(x_0)$ for (a) MJO-B and (b) MJO-C based on the CMAP data, where A is precipitation along MJO tracks averaged in longitudinal bins of x or x_0; x represents 5° longitudinal bins from 100°E to 180°; and x_0 represents the bin of 90°–100°E. Colors indicate the number of events. Dots are the means for each longitudinal bin, and vertical whiskers mark one standard deviation.

A question that arises from Fig. 7 is whether an MJO-C is systematically stronger than an MJO-B before they enter the MC. To address this question, we compared their PDFs of strength, $A(x)$, when their tracks cross 90°E. A similar range of strength exists for both (not shown). Strength is thus not a determining factor to distinguish MJO-C from MJO-B.

As discussed in section 5, MJO-C events do not always have greater zonal scales than MJO-B. We also examined meridional distributions of precipitation as tracks of MJO events cross 90°E but found no discernable sign that may distinguish MJO-C from MJO-B (not shown). We conclude that neither the strength nor size of MJO precipitation before it enters the MC is a critical factor for overcoming the barrier effect.

The barrier effects of the MC are clearly shown in the conventional composite time–longitude diagrams of precipitation anomalies (Fig. 9). Both MJO-B and MJO-C propagate eastward from the Indian Ocean to the MC at a similar averaged speed ($5\,m\,s^{-1}$) with comparable amplitudes and zonal scales of positive anomalies in precipitation. Their amplitudes both substantially decrease immediately after their tracks enter the MC (passing 100°E). This might be a large-scale rain-shadow effect of Sumatra. After that, both quickly recover their strength somewhat, but not to a full extent. Their big difference comes afterward when MJO-B weakens further and quickly vanishes, whereas MJO-C manages to maintain its amplitude in precipitation, however reduced, over the MC and continues moving eastward, with a little hesitation, through the MC into the western Pacific.

A possible explanation for the barrier effect of the MC on the MJO is ENSO. Abnormal subsidence over the MC during a warm episode of ENSO may help weaken MJO convection there. We did not, however, find any obvious connection between the two types of MJO events and the phase of ENSO. Kerns and Chen (2016) found only slight difference in the percentage of MJO-B events between cold or neutral years (40%) and warm years (50%).

There are slightly more MJO-C events (58%) in boreal winter and slightly more MJO-B events (59%) in boreal summer. The propagation patterns of MJO-C events are very different between the two seasons. In boreal winter, MJO-C propagates through the MC via the Java Sea, Banda Sea, and Timor Sea (Fig. 10a). This is typical in boreal winter, when the main MJO activities are south of the equator (Hendon and Salby 1994; Zhang and Dong 2004). In boreal summer, when the main MJO activities are north of the equator, the major passage of

Unauthenticated | Downloaded 12/28/22 07:27 PM UTC

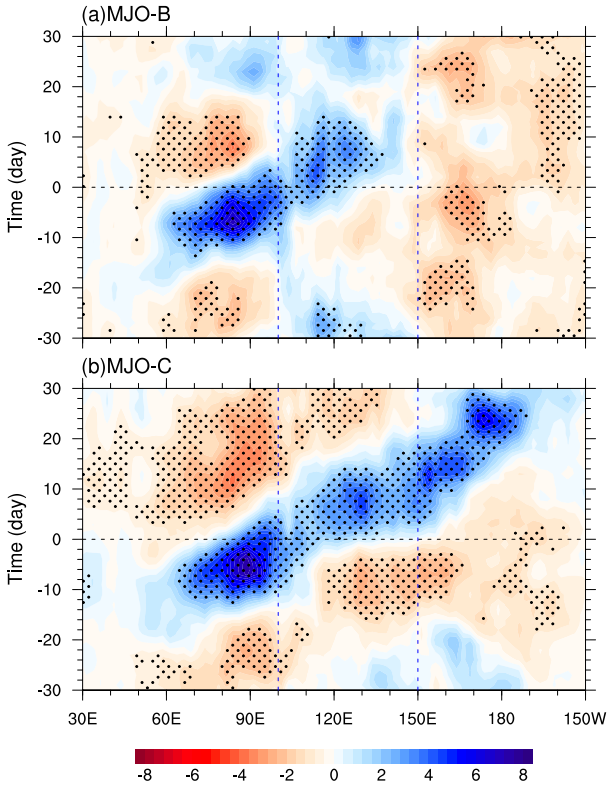

FIG. 9. Composite time–longitude diagrams of precipitation anomalies (mm day^{-1}) averaged over 15°S–15°N for (a) MJO-B and (b) MJO-C based on the CMAP data. Time 0 is when their tracks cross 100°E. Results significant at the 95% confidence level are stippled.

MJO-C through the MC is the South China Sea and Philippine Sea (Fig. 10b). These bifurcated MJO pathways across the MC are nothing new (see, e.g., Wang and Rui 1990; Wu and Hsu 2009). We show this to make two points. First, off-equatorial MJO-C convection projects heavily on the equatorially asymmetric component of the MJO. The diurnal cycle can weaken the asymmetric component as a manifestation of the MC barrier effect, suggested by Tung et al. (2014) and Majda and Yang (2016). Second, MJO-C convection prefers to be over water of the MC, which we will discuss in more detail. Boreal-winter (October–March) MJO events will be the focus in the rest of this article.

There are subtle differences in the evolution of spatial distributions of precipitation between MJO-B and MJO-C when their tracks approach the MC (across 90°E). Precipitation is slightly stronger over the MC, especially over the major islands (Borneo, Sulawesi, and New Guinea) for MJO-C than MJO-B (Figs. 11a,b). We will discuss the possible significance of this subtle difference to the barrier effect in the next subsection. For MJO-B (left column of Fig. 11), large positive anomalies in precipitation move around Borneo on both sides and

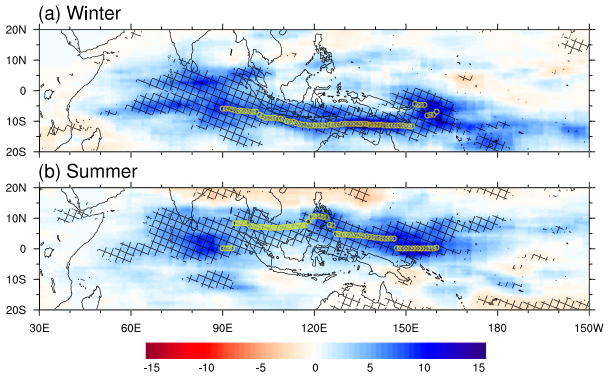

FIG. 10. Composite latitudinal distributions of precipitation anomalies (mm day^{-1}) as a function of longitudes over which tracks of MJO-C pass during boreal (a) winter and (b) summer. Results significant at the 95% confidence level are marked by crosshatching. Latitudinal locations of maximum precipitation anomalies at each longitude grid from 90° to 160°E are marked by yellow circles.

reemerge on the eastern side of the MC near the equator with much-reduced amplitudes. After that, they are further weakened without further eastward motion until they vanish. There is apparent equatorial symmetry in positive anomalies in precipitation for MJO-B, in contrast to MJO-C. As seen in Fig. 10a, eastward-propagating positive precipitation anomalies for MJO-C (right column of Fig. 11) in the MC region are mainly south of the equator, over the Java Sea, Banda Sea, and Timor Sea. After that, its convection center, mainly located south of the equator, continues to move eastward into the SPCZ. Another interesting contrast between the two types of MJO events is their negative anomalies in precipitation west of their convection centers. For MJO-B, a center of negative anomalies in precipitation forms over the western Indian Ocean and moves slowly eastward in tandem with its convection center (positive anomalies in precipitation) until it is over the eastern Indian Ocean, where it stalls as the positive anomalies in precipitation diminish over the MC. For MJO-C, its negative anomalies in precipitation continue to move eastward and penetrate into the MC. One may also notice that, when the convection center is over the MC, the main suppressed convection (negative anomalies in precipitation) is still located over the Indian Ocean for MJO-B, whereas for MJO-C convection is suppressed over both the Indian Ocean and the Pacific.

Next, we compare detailed distributions of precipitation in the MC region for the two types of MJO events.

b. *MJO precipitation over the MC*

There has been observational evidence that convective signals of MJO-C are mainly carried by convection

Unauthenticated | Downloaded 12/28/22 07:27 PM UTC

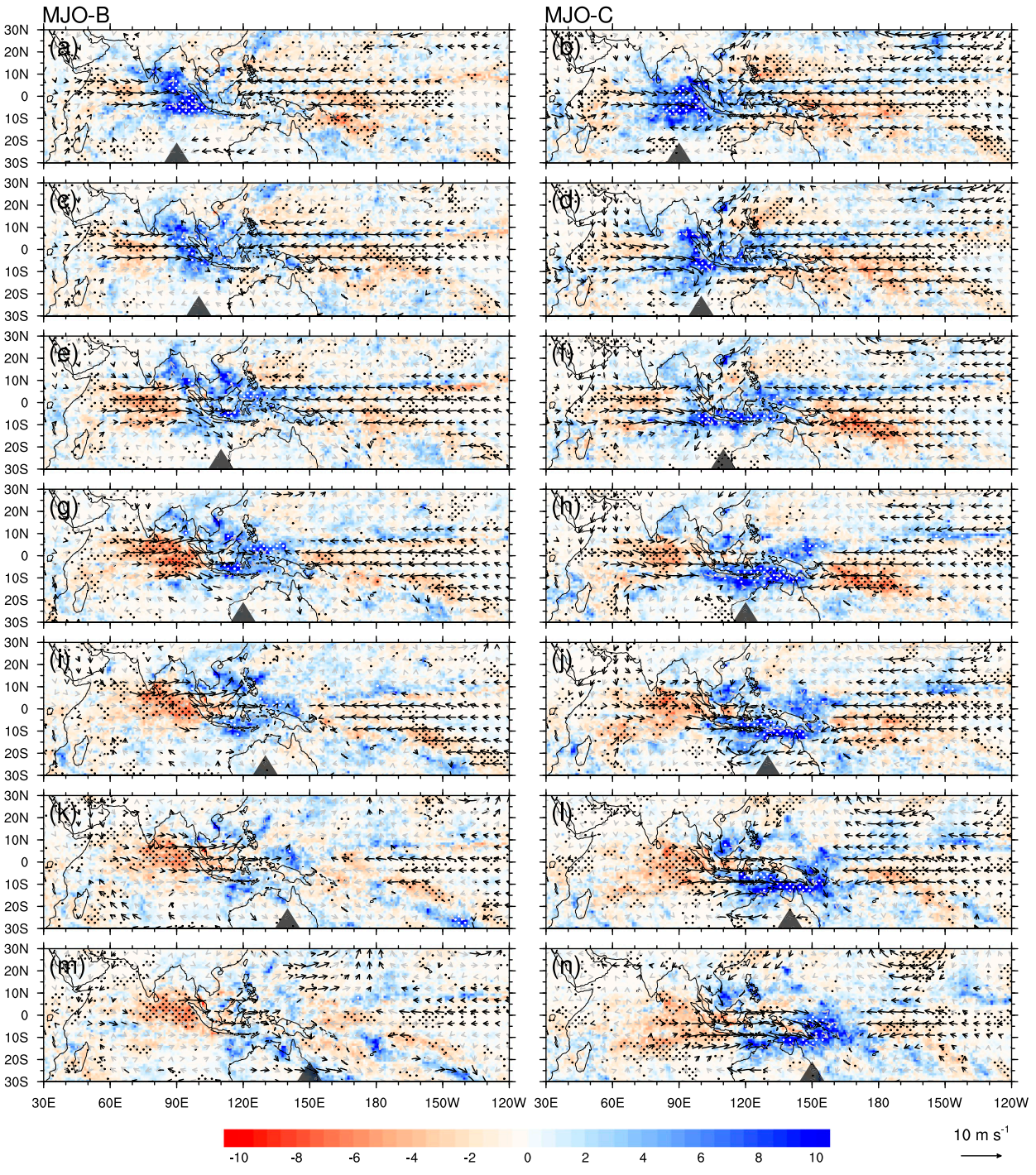

FIG. 11. Composites of anomalies in TRMM precipitation (color shading, mm day^{-1}) and 850-hPa wind vectors from ERA-I for (left) MJO-B and (right) MJO-C when their tracks pass longitudes marked by solid triangles. Stippling for precipitation and thick black vectors for wind mark results significant at the 95% confidence level.

over the sea of the MC (Wu and Hsu 2009). This has nothing to do with the fractional coverage by sea versus land surfaces of the MC (roughly a ratio of 7:3). Mean precipitation over the MC is much higher over land than the sea (Qian 2008; Rauniyar and Walsh 2011). When a convection center of the MJO moves over the MC, there is more convective development over the sea than land in terms of increases in the size and frequency of mesoscale convective systems (MCSs) [Suzuki 2009; also reported by Chen and Kerns (2015)]. Based on this, it is

Unauthenticated | Downloaded 12/28/22 07:27 PM UTC

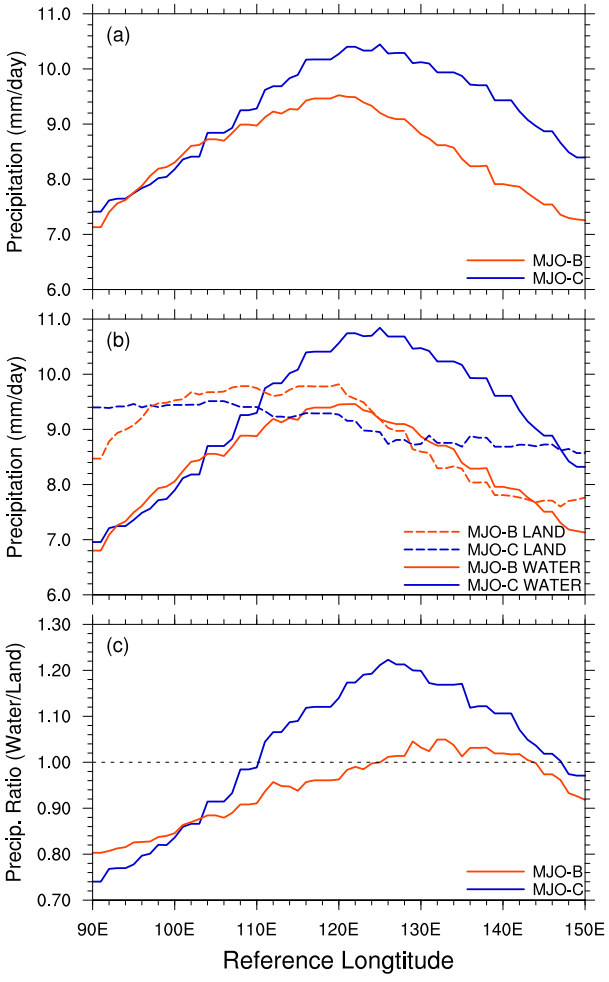

FIG. 12. TRMM precipitation as a function of longitude over which tracks of MJO-C (blue lines) and MJO-B (red lines) pass. (a) Averages over the MC (15°S–15°N, 100°–150°E), (b) averages over the sea (solid lines) and land (dashed lines) of the MC, and (c) ratio of averaged precipitation over the sea to land.

logical to assume that an MJO event would fail to propagate through the MC if its MCSs do not develop sufficiently over the sea of the MC. This is indeed the case.

The evolution of precipitation over the sea and land in the MC is different for MJO-C and MJO-B. Their precipitation averaged over the tropical MC (15°S–15°N, 100°–150°E) increases at a similar pace as their tracks approach the MC from the west (Fig. 12a). Differences between their precipitation amounts emerge after their tracks cross Sumatra (105°E). After that, the mean precipitation of MJO-C over the MC continues to increase first and starts to decay at a slightly later time than that of MJO-B. At their peak times, the mean precipitation of MJO-C is significantly stronger (by 10%) than that of MJO-B. In consequence, even though their mean precipitation decays similarly after their tracks pass 130°E, mean precipitation of MJO-C remains significantly stronger than that of MJO-B.

As convection centers of MJO-B and MJO-C move over the MC, increases in their precipitation in the region take place mainly over the sea (Fig. 12b, solid lines). This increase in precipitation over the sea of the MC is initially at the same pace for both types of the MJO. But it slows down and stops for MJO-B, whereas it continues for MJO-C until its convection centers pass 125°E. The 10% stronger precipitation in the whole MC region for MJO-C in comparison to MJO-B (Fig. 12a) all comes from the difference over the sea. Precipitation averaged over the land of the MC (dashed lines in Fig. 12b) is initially significantly higher than that over the sea for both MJO-B and MJO-C until their tracks cross 110°E. After that, precipitation over the sea becomes significantly stronger than over land for MJO-C, but remains the same for MJO-B. The ratio of precipitation averaged over the sea to land exhibits very different evolution for MJO-B and MJO-C as their tracks move over the MC (Fig. 12c). For MJO-C, land-convection dominance (ratio <1) before its track enters the MC switches to sea-convection dominance when its track is over the MC. For MJO-B, convection over the sea never becomes dominant.

The detailed differential distributions of precipitation over the sea and land of the MC for MJO-B and MJO-C confirm the suspicion that an MJO event is unable to propagate through the MC if its convection fails to fully develop over the sea in the region. Over the open Indian and Pacific Oceans, active MJO convection features wider, deep convection and broad stratiform regions (Morita et al. 2006; Barnes and Houze 2013) than normal. Large MCSs preferably grow over the sea of the MC during the convectively active period of the MJO.[2] This leads to the preference for dominant convection of MJO-C to be over the sea of the MC (Figs. 10, 11).

A possible reason for the failure of oceanic MCS development in the MC is strong landlocked convection. A strong diurnal cycle of land convection is a candidate for the blocking effect on MJO propagation over the MC (Tung et al. 2014; Majda and Yang 2016; Hagos et al. 2016). The strength of the diurnal cycle of land convection might be modulated by the amount of widespread stratiform clouds or saturated ground; both tend to reduce diurnal fluctuations in surface temperature, a main direct diurnal forcing for land convection. Peatman et al. (2014) pointed out a ‘‘vanguard of

[2] This was also reported by Chen and Kerns (2015).

Unauthenticated | Downloaded 12/28/22 07:27 PM UTC

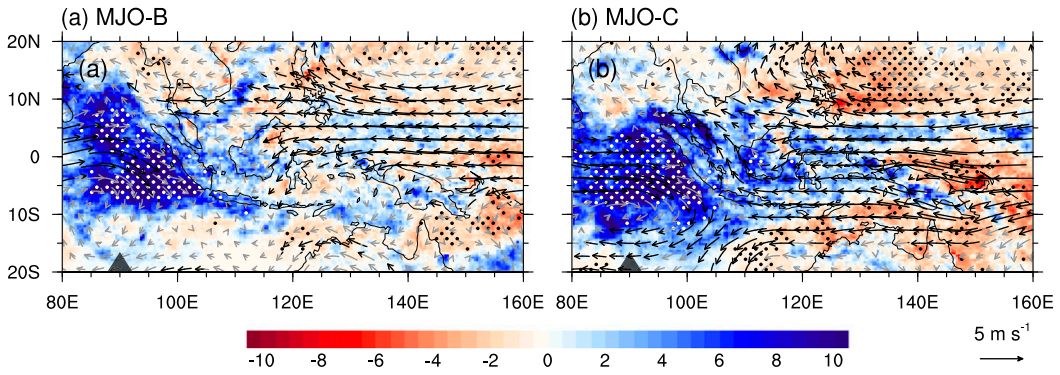

FIG. 13. Enlarged versions of Figs. 11a and 11b, respectively, for the MC.

precipitation'' that increases over land more than over the sea of the MC immediately prior to the arrival of the large-scale convective envelope of the canonical MJO that propagates through the MC. This vanguard of precipitation is more pronounced for MJO-C than MJO-B (Fig. 13). Land precipitation of MJO-C is slightly stronger than that of MJO-B as their tracks pass 90°E (Fig. 12b). This slightly stronger precipitation over land may make the land surface wetter, which would damp surface diurnal forcing of landlocked convection associated with MJO-C when its convection center is over the MC. But this possibility has yet to be explored.

Accompanied to this vanguard of precipitation is stronger, broader (in latitude) low-level (850 hPa) easterly anomalies that penetrate deeper into the MC from the western Pacific for MJO-C in comparison to MJO-B (Fig. 11). In the next subsection, we will explore processes that might be related to the strong easterly anomalies and might provide a reason for a stronger vanguard of precipitation and possibly for overall development of precipitation of MJO-C over the MC.

c. *Large-scale processes*

To seek possible reasons for the stronger vanguard of precipitation for MJO-C, we compare what happens in the MC region immediately before MJO convection centers enter the MC (passing 90°E) when precipitation strengths of MJO-B and MJO-C are similar (Fig. 9). Moisture has been considered one of the most important variables for the MJO (Wang 1988; Raymond and Fuchs 2009; Benedict and Randall 2007; Sobel and Maloney 2013; Adames and Kim 2016). As MJO convection centers approach the MC (their tracks pass 90°E), positive anomalies in lower-tropospheric moisture occur over the MC (not shown). This is consistent with the observed moisture evolution associated with the MJO: low-level moisture increases ahead (east) of MJO convection centers (Hendon and Salby 1994; Jones and Weare 1996; Kiladis et al. 2005; Johnson and Ciesielski 2013). At this time, the positive anomalies in low-level moisture over the MC are different between MJO-C and MJO-B, but only slightly (not shown). It is unknown whether the small, insignificant differences may explain the later different behaviors of the two types of MJO events.

Horizontal distributions of local tendencies of moisture $\partial q/\partial t$ averaged through a layer of 800–500 hPa over the MC do not show significant difference between the two types of MJO events. Local moisture tendencies are small residuals between large-scale moisture flux convergence and apparent moisture sink Q_2 (Yanai et al. 1973) that are almost equal in amplitude but opposite in sign:

$$\frac{\partial q}{\partial t} = -\nabla \cdot (\mathbf{V}q) - \frac{Q_2}{L},$$

where $\mathbf{V}$ is three-dimensional winds, and L is the latent heat of condensation. In general, total moisture flux convergence $-\nabla \cdot (\mathbf{V}q) = -[\partial(uq)/\partial x + \partial(vq)/\partial y + \partial(\omega q)/\partial p]$ provides a large-scale source of moisture, and moisture is removed from the atmosphere by precipitation through microphysical processes represented by Q_2. The differential behaviors between the vanguard of precipitation of MJO-B and MJO-C might result from the large-scale moisture sources over the MC.

Total moisture flux convergence averaged through a layer of 850–500 hPa over the MC does not exhibit significant differences between MJO-B and MJO-C as their convection centers approach the MC (not shown). However, its vertical structures, especially those of its individual components, do. This is demonstrated in a longitude–vertical cross section (Fig. 14) and, more obviously, in a latitude–vertical cross section (Fig. 15). For MJO-C, there is low-level moisture flux convergence over the MC east of Sumatra (Fig. 14b), which is contributed by its zonal component $-\partial(uq)/\partial x$, with a deep (from the surface to the 500–400-hPa level) easterly anomalies to the east and westerly anomalies to the west (Fig. 14d). In comparison, for MJO-B, the lower-tropospheric easterly anomalies are significantly

Unauthenticated | Downloaded 12/28/22 07:27 PM UTC

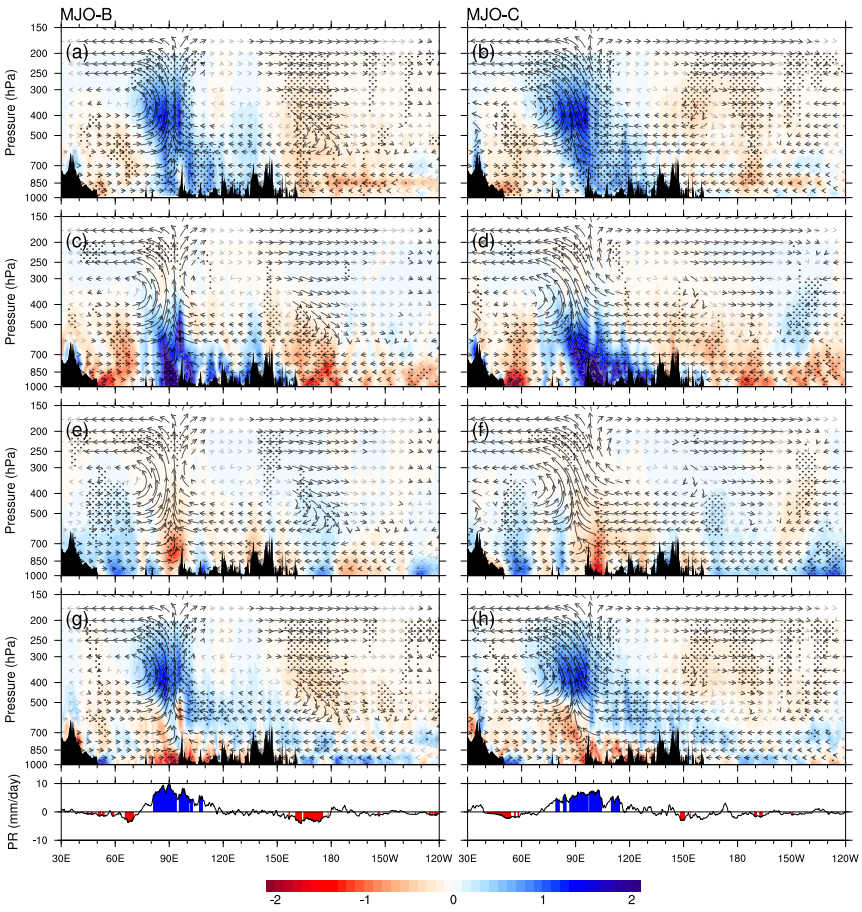

FIG. 14. Composites of zonal–vertical distributions of anomalous wind vectors (u, ω) overlaid with (a),(b) total moisture flux convergence and its (c),(d) zonal, (e),(f) meridional, and (g),(h) vertical components (color shading; 10^{-5} g kg^{-1} s^{-1}), all averaged over 10°S–10°N, for (left) MJO-B and (right) MJO-C when their tracks pass 90°E. (bottom) Curves for correspondingly averaged precipitation (mm day^{-1}). Results significant at the 95% confidence level are marked by black arrows for wind vectors, stippling for moisture flux convergence, and color for precipitation. Black shading at the bottom of each panel indicates the averaged height of the terrain. Vertical velocities are scaled by a factor of 250 to make them visible.

weaker, leading to weaker low-level moisture flux convergence by the zonal component over the MC between Sumatra and New Guinea (Fig. 14c). The meridional component $-\partial(vq)/\partial y$ of MJO-C offsets the zonal moisture flux convergence by producing divergence, especially at the eastern side of Sumatra (Fig. 14f), which shifts to the western side for MJO-B (Fig. 14e). The vertical component $-\partial(\omega q)/\partial p$ provides moisture flux divergence in the lowest level and convergence aloft (Figs. 14g,h), implying an upward moisture transport. There is a sign of a gradual deepening of low-level moisture flux convergence from the east to west over the MC for MJO-C (Fig. 14h). This implies a systematic increase in the depth of convection toward the convection center, which has been observed for most MJO events over the open oceans (Lau and Wu 2010; Del Genio et al. 2012; Powell and Houze 2013; Xu and Rutledge 2014). This also happens to MJO-B but to a lesser degree.

Differences between the vertical structure of moisture flux convergence of MJO-C and MJO-B are more evident in a meridional–vertical cross section (Fig. 15). For MJO-B, there is a cross-equatorial flow extending from near the surface to the midtroposphere (Fig. 15a). For MJO-C, the meridional flow is almost equatorially symmetric, with poleward flows on both sides of the equator through the entire lower-to-middle troposphere (Fig. 15b). Moisture flux convergence by the zonal component (Figs. 15c,d) and divergence by the meridional component (Figs. 15e,f) are evidently stronger for MJO-C than for MJO-B, which can be seen in the zonal–vertical cross sections (Fig. 14). Midtropospheric moisture flux convergence by the

Unauthenticated | Downloaded 12/28/22 07:27 PM UTC

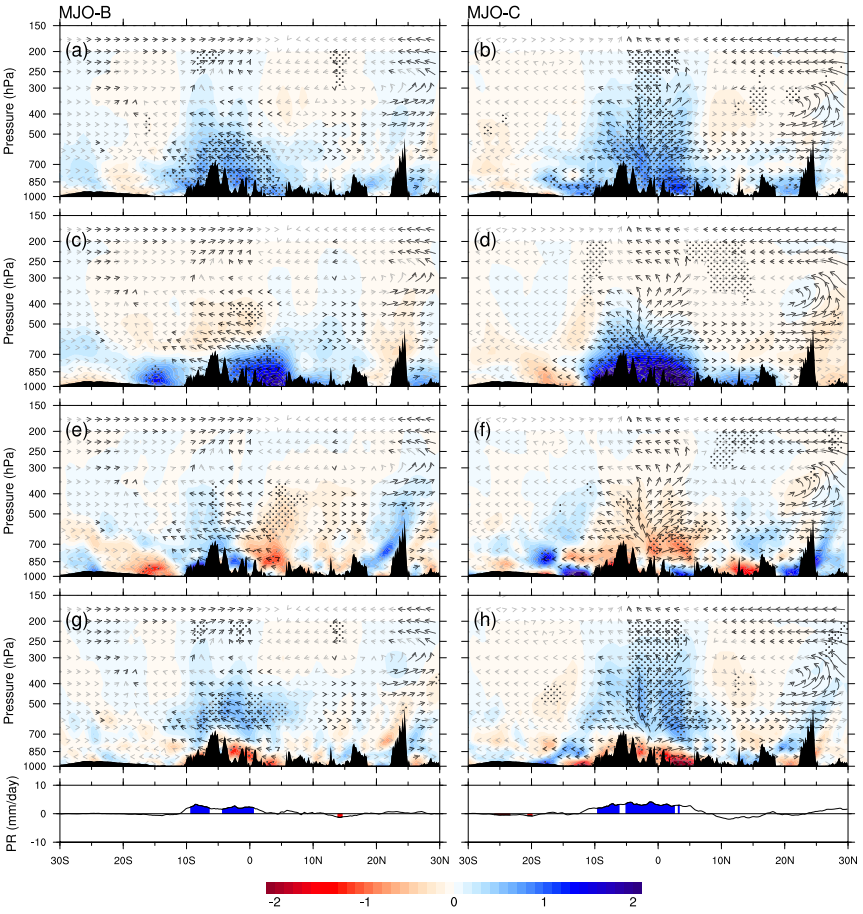

FIG. 15. As in Fig. 14, but for meridional–vertical distributions of anomalous wind vectors (v, ω) overlaid with the same moisture flux convergence components averaged over 100°–130°E.

vertical component is much higher for MJO-C (Fig. 15h) than for MJO-B (Fig. 15g).

The major difference between MJO-C and MJO-B in their moisture flux convergence over the MC is summarized in Fig. 16, which shows profiles of each component and the total averaged over 100°–130°E and 10°S–10°N when MJO convection centers are at 90°E. There is no significant difference in the total moisture flux convergence. Profiles of the moisture sink Q_2 are very similar to those of the total moisture flux convergence, but with the opposite sign, leading to the local moisture tendency being an order of magnitude smaller. Detailed diagnostics of moisture budget can be done using an approach emphasizing the ''column confined'' process (Chikira 2014; Janiga and Zhang 2016). This approach requires information of radiative and cumulus diabatic heating, which is not available from the global reanalysis used here. The contrasting circulation patterns and strength of MJO-C and MJO-B deserve further investigation. There is no significant difference in the vertical structure of the apparent heating Q_1 between MJO-B and MJO-C (not shown). The Q_1 distribution in the meridional direction is wider for MJO-C than MJO-B, consistent with their precipitation distributions (Fig. 15).

Possible effects of sea surface temperature (SST) on the MJO have been demonstrated using observations and numerical models [see a review on this subject by DeMott et al. (2015)]. As an MJO track approaches the MC, SST in the southern part of the MC (the eastern Indian Ocean south of Java, the Banda Sea, and the Timor Sea) is significantly higher for MJO-C than MJO-B (Fig. 17). There, observed intraseasonal fluctuations in SST are the strongest in the MC (Napitu et al. 2015). Meanwhile, the equatorial SST east of the Pacific warm pool (150°E–180°) is significantly lower for MJO-B than for MJO-C.

The high SST in the southern part of the MC for MJO-C does not appear to be explainable in terms of surface energy flux. Surface wind is actually stronger

Unauthenticated | Downloaded 12/28/22 07:27 PM UTC

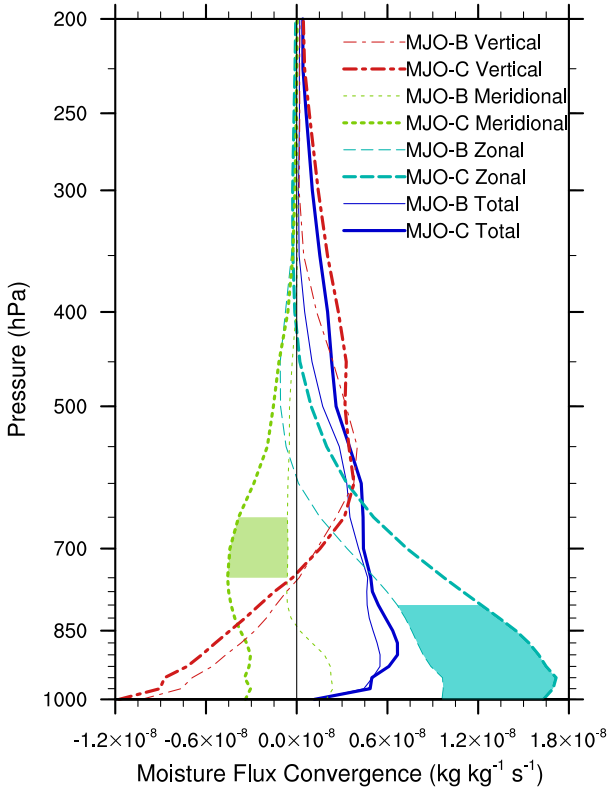

FIG. 16. Composites of vertical profiles of anomalous total moisture flux convergence and its zonal, meridional, and vertical components, all averaged over 10°S–10°N, 100°–130°E for MJO-B and MJO-C when their tracks pass 90°E. Shadings mark their differences significant at the 95% confidence level.

where SST is higher. Compared to MJO-B, surface evaporation is slightly lower and total surface energy flux into the ocean is higher for MJO-C in the Timor Sea and eastern Indian Ocean immediately south of Java, but it is the opposite in the Banda Sea (not shown). This suggests that oceanic processes (e.g., tidal mixing and advection) need to be considered to explain the difference in SST between MJO-C and MJO-B.

7. Summary, discussion, and concluding remarks

In this study, we have applied a precipitation-tracking method to identify MJO events and distinguish those that propagate across the MC (MJO-C) from those that are blocked by the MC (MJO-B). The main advantage of this method is its ability to determine quantitatively characteristics of individual MJO events that cannot be derived from methods based on EOF analysis (Wheeler and Hendon 2004; Kiladis et al. 2014; Liu et al. 2016). This method reveals that 60% of all MJO events and most strong MJO events form over the Indian Ocean between 30° and 100°E. The weakest MJO events mostly form outside the Indian Ocean. MJO events with larger zonal scales tend to propagate over longer distance. These and other characteristics of the MJO were used to quantify the barrier effect of the MC. Consistent results were obtained using the TRMM (1998–2015) and CMAP (1979–2014) precipitation data. The results are robust in the sense that they remain qualitatively the same as the criteria that have to be determined a priori for the tracking method vary slightly.

The two peaks in the zonal distribution of ending longitudes of the MJO (Fig. 5) unambiguously demonstrate the barrier effect of the MC that blocks about a half of MJO events formed over the Indian Ocean from propagating through. For the other half that propagates through, most of them (>75%) become weakened over the MC (Fig. 6). The barrier effect cannot be explained in terms of the strength and horizontal scale or distributions of MJO convection centers when they approach the MC from the west. A main distinction between MJO-B and MJO-C is their precipitation over the sea versus land in the MC region. MJO events may propagate through the MC only when their convection over

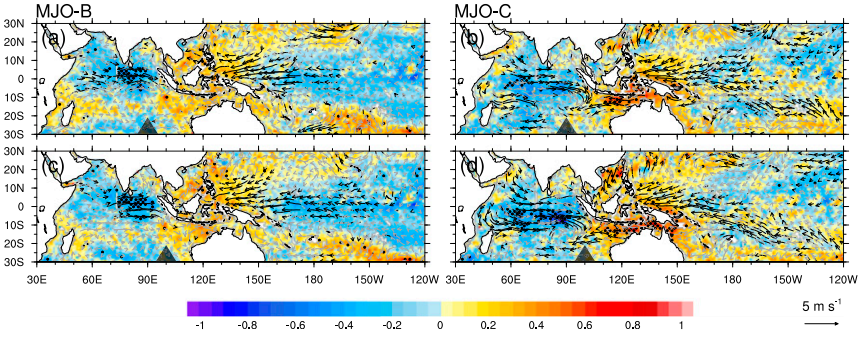

FIG. 17. Composites of anomalies in SST (color shading; °C) and TMI surface wind vectors for (a),(c) MJO-B and (b),(d) MJO-C when their tracks pass (top) 90°E and (bottom) 100°E (marked by solid triangles) based on the TRMM precipitation data. Stippling for SST and thick black vectors for wind mark results significant at the 95% confidence level.

Unauthenticated | Downloaded 12/28/22 07:27 PM UTC

the sea of the MC is sufficiently developed and dominates that over land; when land-convection dominance persists over the MC, MJO events would fail to propagate through (Fig. 12). The MC barrier effect on MJO propagation is thus to discourage MJO convection from developing over the sea of the MC.

We have attempted to explain this barrier effect of the MC based on the recent work of Tung et al. (2014), Majda and Yang (2016), and Hagos et al. (2016). Using global data, a theoretical model, and a regional cloud-permitting model, respectively, they reached a conclusion that the landlocked convective diurnal cycle can be detrimental to MJO propagation through the MC. If this is true, and if dominant landlocked diurnal convection compromises the development of convection over the sea of the MC, then damping diurnal forcing over land may help overcome the barrier effect. One way to damp diurnal forcing of land is to increase land surface moisture. We hypothesize that this is accomplished by the vanguard of precipitation over land (Peatman et al. 2014) that is slightly stronger for MJO-C than for MJO-B when their convection centers are immediately west of the MC (Figs. 12b, 13). Seeking reasons behind the stronger vanguard of precipitation for MJO-C, we explored whether moisture flux convergence over the MC and SST of the MC seas might be factors. As MJO convection centers approach the MC, there are significant differences between MJO-C and MJO-B in their low-level zonal and meridional moisture convergence over the MC, even though little difference exists in their total moisture convergence (Figs. 14–16). We also found significant differences between MJO-C and MJO-B in SST over the Java Sea, Benda Sea, and Timor Sea (Fig. 17). This part of the results is qualitative and inclusive. Instead of providing convincing explanations for the barrier effect, these results point to possible targets of future research.

In the introduction of this article, we proposed two criteria that any explanation for the barrier effect of the MC on the MJO should meet. The first one is that such an explanation should include specific features of the MC: its intricate land–sea distributions and elevated terrains. The second is that it should include mechanisms for both the barrier effect and its overcoming by some MJO events. In this study, the explanation for the barrier effect in terms of the precipitation distributions over the sea versus land of the MC satisfies the first criterion. The diagnostics of moisture flux convergence and SST in the MC were produced to satisfy the second.

This study presents quantitative information about the MC barrier effect on the MJO but does not reach a complete and satisfactory explanation for the barrier effect and its overcoming by some MJO events. Much still needs to be done to close the loose ends of our hypothesized chain of processes involved with the distribution of land versus sea convection, landlocked diurnal convection, and damping of land diurnal forcing by the vanguard of precipitation. Because of the coarse temporal resolution of current observations, it is impossible to evaluate the role of the diurnal cycle in the relationship between the large-scale moisture convergence and precipitation over MC in the current study. To fill the gaps, we propose that the following research topics be pursued to advance our understanding of the barrier effect of the MC:

1) Interactions of convective systems over the sea and land of the MC under different large-scale condition: It is unknown how much of the MJO-C convection development over the sea is related to offshore propagation of convection initiated over land (Houze et al. 1981; Mori et al. 2004; Keenan and Carbone 2008) and how much is initiated over the water. While offshore propagation and land–sea breezes dictate diurnal precipitation over the MC (Hashiguchi et al. 1995; Hadi et al. 2002; Sakurai et al. 2005; Araki et al. 2006; Zhou and Wang 2006; Tabata et al. 2011), it is unclear what other processes may also be instrumental to the interaction of convection over the sea and land. It is also unknown if landlocked diurnal convection tends to suppress convection over the adjacent seas as we hypothesized and what processes (e.g., competing for moisture and creating stronger offshore surface divergence) might be involved.
2) Orographic effect on large-scale moisture flux convergence: This depends on the direction as well as strength of low-level winds. Detailed behaviors of MJO convection and its associated large-scale conditions around and over elevated terrains have been documented using EOF-based MJO indices (Hsu and Lee 2005; Wu and Hsu 2009). They should be reproduced using tracking-based methods (Kerns and Chen 2016; this study).
3) Processes controlling SST and air–sea interaction in the MC: The observed higher SST in the MC region for MJO-C cannot be explained by larger energy flux into the ocean. Upper-ocean processes are likely to be involved. Mixing under influences of bathymetry, tides, river runoff, and the Indonesian Throughflow is unique to the MC in comparison to the open oceans. For example, as discussed in Sprintall et al. (2014) and Koch-Larrouy et al. (2015), tidal mixing can modify the SST of the MC by 0.5°C. With the adjacent land, the sensitivity of marine convection to SST is presumably different from that over the open

Unauthenticated | Downloaded 12/28/22 07:27 PM UTC

ocean. This sensitivity is intertwined with the land–sea breezes that also depend on SST.

It is possible and even plausible that the barrier effect of the MC on the MJO is multifaceted, with more than one mechanisms acting individually or interactively. The results from this study, especially the difference in precipitation over the sea and land in the MC between MJO events that propagate through the MC and those that do not, suggest that complete understanding of the barrier effect should be based on thorough knowledge of detailed processes in situ to the MC. Such knowledge can be acquired through studies using a combination of field observations, high-resolution data assimilation products, and high-resolution model simulations. Information to be collected by the joint research emphasis on understanding MJO interactions with the Maritime Continent [organized by the Subseasonal-to-Seasonal (S2S) Prediction Project and MJO Task Force] and by the international program Years of the Maritime Continent (YMC; 2017–19) will play irreplaceable roles in advancing the study on the barrier effect of the MC on the MJO.

Acknowledgments. The authors thank Kyong-Hwan Seo and two anonymous reviewers for their constructive comments on an earlier version of this article. A code of precipitation tracking in NCL is available for anyone who is interested in using it. This research is sponsored by the National Basic Research Program of China through Grant 2015CB453200; the National Natural Science Foundation of China through Grants 41575062 and 41520104008; the Key Research Program of Frontier Sciences of CAS through Grant QYZDB-SSW-DQC017 (JL); and by NOAA Grant NA13OAR4310161 through the Climate Variability and Prediction Program of the Climate Program Office (CZ).

REFERENCES

Adames, A. F., and M. Wallace, 2014: Three-dimensional structure and evolution of the MJO and its relation to the mean flow. *J. Atmos. Sci.*, **71**, 4661–4681, doi:10.1175/JAS-D-14-0091.1.

——, and D. Kim, 2016: The MJO as a dispersive, convectively coupled moisture wave: Theory and observations. *J. Atmos. Sci.*, **73**, 913–941, doi:10.1175/JAS-D-15-0170.1.

Araki, R., M. D. Yamanaka, F. Murata, H. Hashiguchi, Y. Oku, T. Sribimawati, M. Kudsy, and F. Renggono, 2006: Seasonal and interannual variations of diurnal cycles of wind and cloud activity observed at Serpong, West Jawa, Indonesia. *J. Meteor. Soc. Japan*, **84A**, 171–194, doi:10.2151/jmsj.84A.171.

Barnes, H. C., and R. A. Houze Jr., 2013: The precipitating cloud population of the Madden–Julian oscillation over the Indian and west Pacific Oceans. *J. Geophys. Res. Atmos.*, **118**, 6996–7023, doi:10.1002/jgrd.50375.

Benedict, J. J., and D. A. Randall, 2007: Observed characteristics of the MJO relative to maximum rainfall. *J. Atmos. Sci.*, **64**, 2332–2354, doi:10.1175/JAS3968.1.

Chen, S., and B. Kerns, 2015: Diurnal cycle of convective cloud systems over the Maritime Continent and its variability during MJO. *2015 Fall Meeting*, San Francisco, CA, Amer. Geophys. Union, Abstract A22E-03. [Available online at https://agu.confex.com/agu/fm15/webprogram/Paper77584.html.]

Chikira, M., 2014: Eastward-propagating intraseasonal oscillation represented by Chikira–Sugiyama cumulus parameterization. Part II: Understanding moisture variation under weak temperature gradient balance. *J. Atmos. Sci.*, **71**, 615–639, doi:10.1175/JAS-D-13-038.1.

Dee, D. P., and Coauthors, 2011: The ERA-Interim reanalysis: Configuration and performance of the data assimilation system. *Quart. J. Roy. Meteor. Soc.*, **137**, 553–597, doi:10.1002/qj.828.

Del Genio, A. D., Y. Chen, D. Kim, and M.-S. Yao, 2012: The MJO transition from shallow to deep convection in CloudSat/CALIPSO data and GISS GCM simulations. *J. Climate*, **25**, 3755–3770, doi:10.1175/JCLI-D-11-00384.1.

DeMott, C. A., N. P. Klingaman, and S. J. Woolnough, 2015: Atmosphere–ocean coupled processes in the Madden–Julian oscillation. *Rev. Geophys.*, **53**, 1099–1154, doi:10.1002/2014RG000478.

Dole, R., and Coauthors, 2014: The making of an extreme event: Putting the pieces together. *Bull. Amer. Meteor. Soc.*, **95**, 427–440, doi:10.1175/BAMS-D-12-00069.1.

Feng, J., T. Li, and W. Zhu, 2015: Propagating and nonpropagating MJO events over Maritime Continent. *J. Climate*, **28**, 8430–8449, doi:10.1175/JCLI-D-15-0085.1.

Fu, X., J. Y. Lee, B. Wang, W. Wang, and F. Vitart, 2013: Intraseasonal forecasting of the Asian summer monsoon in four operational and research models. *J. Climate*, **26**, 4186–4203, doi:10.1175/JCLI-D-12-00252.1.

Gaiser, P. W., and Coauthors, 2004: The WindSat spaceborne polarimetric microwave radiometer: Sensor description and early orbit performance. *IEEE Trans. Geosci. Remote Sens.*, **42**, 2347–2361, doi:10.1109/TGRS.2004.836867.

Gentemann, C. L., T. Meissner, and F. J. Wentz, 2010: Accuracy of satellite sea surface temperatures at 7 and 11 GHz. *IEEE Trans. Geosci. Remote Sens.*, **48**, 1009–1018, doi:10.1109/TGRS.2009.2030322.

Gottschalck, J., P. E. Roundy, C. J. Schreck, A. Vintzileos, and C. D. Zhang, 2013: Large-scale atmospheric and oceanic conditions during the 2011–12 DYNAMO field campaign. *Mon. Wea. Rev.*, **141**, 4173–4196, doi:10.1175/MWR-D-13-00022.1.

Hadi, T. W., T. Horinouchi, T. Tsuda, H. Hashiguchi, and S. Fukao, 2002: Sea-breeze circulation over Jakarta, Indonesia: A climatology based on boundary layer radar observations. *Mon. Wea. Rev.*, **130**, 2153–2166, doi:10.1175/1520-0493(2002)130<2153:SBCOJI>2.0.CO;2.

Hagos, S. M., C. Zhang, Z. Feng, C. D. Burleyson, C. De Mott, B. Kerns, J. J. Benedict, and M. N. Martini, 2016: The impact of the diurnal cycle on the propagation of Madden–Julian oscillation convection across the Maritime Continent. *J. Adv. Model. Earth Syst.*, **8**, 1552–1564, doi:10.1002/2016MS000725.

Hashiguchi, H., M. D. Yamanaka, and T. Tsuda, 1995: Diurnal-variations of the planetary boundary-layer observed with an L-band clear-air Doppler radar. *Bound.-Layer Meteor.*, **74**, 419–424, doi:10.1007/BF00712381.

Hendon, H. H., and M. L. Salby, 1994: The life cycle of the Madden–Julian oscillation. *J. Atmos. Sci.*, **51**, 2225–2237, doi:10.1175/1520-0469(1994)051<2225:TLCOTM>2.0.CO;2.

Unauthenticated | Downloaded 12/28/22 07:27 PM UTC

——, B. Liebmann, M. E. Newman, J. D. Glick, and J. E. Schemm, 2000: Medium range forecasts errors associated with active episodes of the Madden–Julian oscillation. *Mon. Wea. Rev.*, **128**, 69–86, doi:10.1175/1520-0493(2000)128<0069:MRFEAW>2.0.CO;2.

Hoffman, R. N., and S. M. Leidner, 2005: An introduction to the near-real-time QuikSCAT data. *Wea. Forecasting*, **20**, 476–493, doi:10.1175/WAF841.1.

Houze, R. A., Jr., S. G. Geotis, F. D. Marks, and A. K. West, 1981: Winter monsoon convection in the vicinity of North Borneo. Part I: Structure and time variation of the clouds and precipitation. *Mon. Wea. Rev.*, **109**, 1595–1614, doi:10.1175/1520-0493(1981)109<1595:WMCITV>2.0.CO;2.

Hsu, H.-H., and M. Y. Lee, 2005: Topographic effects on the eastward propagation and initiation of the Madden–Julian oscillation. *J. Climate*, **18**, 795–809, doi:10.1175/JCLI-3292.1.

Hu, Q., and D. A. Randall, 1994: Low-frequency oscillations in radiative-convective systems. *J. Atmos. Sci.*, **51**, 1089–1099, doi:10.1175/1520-0469(1994)051<1089:LFOIRC>2.0.CO;2.

——, and ——, 1995: Low-frequency oscillations in radiative-convective systems. Part II: An idealized model. *J. Atmos. Sci.*, **52**, 478–490, doi:10.1175/1520-0469(1995)052<0478:LFOIRC>2.0.CO;2.

Huffman, G. J., and Coauthors, 2007: The TRMM Multisatellite Precipitation Analysis (TMPA): Quasi-global, multiyear, combined-sensor precipitation estimates at fine scales. *J. Hydrometeor.*, **8**, 38–55, doi:10.1175/JHM560.1.

Inness, P. M., and J. M. Slingo, 2003: Simulation of the Madden–Julian oscillation in a coupled general circulation model. Part I: Comparisons with observations and an atmosphere-only GCM. *J. Climate*, **16**, 345–364, doi:10.1175/1520-0442(2003)016<0345:SOTMJO>2.0.CO;2.

——, and ——, 2006: The interaction of the Madden–Julian oscillation with the Maritime Continent in a GCM. *Quart. J. Roy. Meteor. Soc.*, **132**, 1645–1667, doi:10.1256/qj.05.102.

Janiga, M. A., and C. Zhang, 2016: MJO moisture budget during DYNAMO in a cloud-permitting model. *J. Atmos. Sci.*, **73**, 2257–2278, doi:10.1175/JAS-D-14-0379.1.

Johnson, R. H., and P. E. Ciesielski, 2013: Structure and properties of Madden–Julian oscillations deduced from DYNAMO sounding arrays. *J. Atmos. Sci.*, **70**, 3157–3179, doi:10.1175/JAS-D-13-065.1.

Jones, C., and B. C. Weare, 1996: The role of low-level moisture convergence and ocean latent heat flux in the Madden–Julian oscillation: An observational analysis using ISCCP data and ECMWF analyses. *J. Climate*, **9**, 3086–3104, doi:10.1175/1520-0442(1996)009<3086:TROLLM>2.0.CO;2.

Keenan, T. D., and R. E. Carbone, 2008: Propagation and diurnal evolution of warm season cloudiness in the Australian and Maritime Continent region. *Mon. Wea. Rev.*, **136**, 973–994, doi:10.1175/2007MWR2152.1.

Kerns, B. W., and S. S. Chen, 2016: Large-scale precipitation tracking and the MJO over the Maritime Continent and Indo-Pacific warm pool. *J. Geophys. Res. Atmos.*, **121**, 8755–8776, doi:10.1002/2015JD024661.

Kiladis, G. N., K. H. Straub, and P. T. Haertel, 2005: Zonal and vertical structure of the Madden–Julian oscillation. *J. Atmos. Sci.*, **62**, 2790–2809, doi:10.1175/JAS3520.1.

——, J. Dias, K. H. Straub, M. C. Wheeler, S. N. Tulich, K. Kikuchi, K. M. Weickmann, and M. J. Ventrice, 2014: A comparison of OLR and circulation-based indices for tracking the MJO. *Mon. Wea. Rev.*, **142**, 1697–1715, doi:10.1175/MWR-D-13-00301.1.

Kim, D., and Coauthors, 2009: Application of MJO simulation diagnostics to climate models. *J. Climate*, **22**, 6413–6436, doi:10.1175/2009JCLI3063.1.

——, J. S. Kug, and A. H. Sobel, 2014: Propagating versus nonpropagating Madden–Julian oscillation events. *J. Climate*, **27**, 111–125, doi:10.1175/JCLI-D-13-00084.1.

Kim, H. M., D. Kim, F. Vitart, V. E. Toma, J. S. Kug, and P. J. Webster, 2016: MJO propagation across the Maritime Continent in the ECMWF ensemble prediction system. *J. Climate*, **29**, 3973–3988, doi:10.1175/JCLI-D-15-0862.1.

Koch-Larrouy, A., A. Atmadipoera, P. van Beek, G. Madec, J. Aucan, F. Lyard, J. Grelet, and M. Souhaut, 2015: Estimates of tidal mixing in the Indonesian archipelago from multidisciplinary INDOMIX in-situ data. *Deep-Sea Res. I*, **106**, 136–153, doi:10.1016/j.dsr.2015.09.007.

Lafleur, D. M., B. S. Barrett, and G. R. Henderson, 2015: Some climatological aspects of the Madden–Julian oscillation (MJO). *J. Climate*, **28**, 6039–6053, doi:10.1175/JCLI-D-14-00744.1.

Lau, K.-M., and H.-T. Wu, 2010: Characteristics of precipitation, cloud, and latent heating associated with the Madden–Julian oscillation. *J. Climate*, **23**, 504–518, doi:10.1175/2009JCLI2920.1.

Ling, J., P. Bauer, P. Bechtold, A. Beljaars, R. Forbes, F. Vitart, M. Ulate, and C. D. Zhang, 2014: Global versus local MJO forecast skill of the ECMWF model during DYNAMO. *Mon. Wea. Rev.*, **142**, 2228–2247, doi:10.1175/MWR-D-13-00292.1.

Liu, P., Q. Zhang, C. Zhang, Y. Zhu, M. Khairoutdinov, H. M. Kim, C. Schumacher, and M. Zhang, 2016: A revised real-time multivariate MJO index. *Mon. Wea. Rev.*, **144**, 627–642, doi:10.1175/MWR-D-15-0237.1.

Madden, R. A., and P. R. Julian, 1971: Detection of a 40–50-day oscillation in zonal wind in tropical Pacific. *J. Atmos. Sci.*, **28**, 702–708, doi:10.1175/1520-0469(1971)028<0702:DOADOI>2.0.CO;2.

——, and ——, 1972: Description of global-scale circulation cells in tropics with a 40–50 day period. *J. Atmos. Sci.*, **29**, 1109–1123, doi:10.1175/1520-0469(1972)029<1109:DOGSCC>2.0.CO;2.

Majda, A. J., and Q. Yang, 2016: A multiscale model for the intraseasonal impact of the diurnal cycle over the Maritime Continent on the Madden–Julian oscillation. *J. Atmos. Sci.*, **73**, 579–604, doi:10.1175/JAS-D-15-0158.1.

Maloney, E. D., and A. H. Sobel, 2004: Surface fluxes and ocean coupling in the tropical intraseasonal oscillation. *J. Climate*, **17**, 4368–4386, doi:10.1175/JCLI-3212.1.

Matthews, A. J., 2008: Primary and successive events in the Madden–Julian oscillation. *Quart. J. Roy. Meteor. Soc.*, **134**, 439–453, doi:10.1002/qj.224.

Mori, S., and Coauthors, 2004: Diurnal land–sea rainfall peak migration over Sumatera Island, Indonesian Maritime Continent observed by TRMM satellite and intensive rawinsonde soundings. *Mon. Wea. Rev.*, **132**, 2021–2039, doi:10.1175/1520-0493(2004)132<2021:DLRPMO>2.0.CO;2.

Morita, J., Y. N. Takayabu, S. Shige, and Y. Kodama, 2006: Analysis of rainfall characteristics of the Madden–Julian oscillation using TRMM satellite data. *Dyn. Atmos. Oceans*, **42**, 107–126, doi:10.1016/j.dynatmoce.2006.02.002.

Napitu, A. M., A. L. Gordon, and K. Pujiana, 2015: Intraseasonal sea surface temperature variability across the Indonesian seas. *J. Atmos. Sci.*, **28**, 8710–8727, doi:10.1175/JCLI-D-14-00758.1.

Neale, R., and J. Slingo, 2003: The Maritime Continent and its role in the global climate: A GCM study. *J. Climate*, **16**, 834–848, doi:10.1175/1520-0442(2003)016<0834:TMCAIR>2.0.CO;2.

Unauthenticated | Downloaded 12/28/22 07:27 PM UTC

Peatman, S. C., A. J. Matthews, and D. P. Stevens, 2014: Propagation of the Madden–Julian oscillation through the Maritime Continent and scale interaction with the diurnal cycle of precipitation. *Quart. J. Roy. Meteor. Soc.*, **140**, 814–825, doi:10.1002/qj.2161.

Powell, S. W., and R. A. Houze Jr., 2013: The cloud population and onset of the Madden–Julian oscillation over the Indian Ocean during DYNAMO-AMIE. *J. Geophys. Res. Atmos.*, **118**, 11 979–11 995, doi:10.1002/2013JD020421.

Qian, J. H., 2008: Why precipitation is mostly concentrated over islands in the Maritime Continent. *J. Atmos. Sci.*, **65**, 1428–1441, doi:10.1175/2007JAS2422.1.

Rauniyar, S. P., and K. J. E. Walsh, 2011: Scale interaction of the diurnal cycle of rainfall over the Maritime Continent and Australia: Influence of the MJO. *J. Climate*, **24**, 325–348, doi:10.1175/2010JCLI3673.1.

Raymond, D. J., and Z. Fuchs, 2009: Moisture modes and the Madden–Julian oscillation. *J. Climate*, **22**, 3031–3046, doi:10.1175/2008JCLI2739.1.

Roundy, P. E., 2012: The spectrum of convectively coupled Kelvin waves and the Madden–Julian oscillation in regions of low-level easterly and westerly background flow. *J. Atmos. Sci.*, **69**, 2107–2111, doi:10.1175/JAS-D-12-060.1.

——, C. J. Schreck III, and M. A. Janiga, 2009: Contributions of convectively coupled equatorial Rossby waves and Kelvin waves to the real-time multivariate MJO indices. *Mon. Wea. Rev.*, **137**, 469–478, doi:10.1175/2008MWR2595.1.

Rui, H., and B. Wang, 1990: Development characteristics and dynamic structure of tropical intraseasonal convection anomalies. *J. Atmos. Sci.*, **47**, 357–379, doi:10.1175/1520-0469(1990)047<0357:DCADSO>2.0.CO;2.

Sakurai, N., and Coauthors, 2005: Diurnal cycle of cloud system migration over Sumatera Island. *J. Meteor. Soc. Japan*, **83**, 835–850, doi:10.2151/jmsj.83.835.

Seo, K.-H., W. Wang, J. Gottschalck, Q. Zhang, J.-K. E. Schemm, W. R. Higgins, and A. Kumar, 2009: Evaluation of MJO forecast skill from several statistical and dynamical forecast models. *J. Climate*, **22**, 2372–2388, doi:10.1175/2008JCLI2421.1.

Sobel, A., and E. Maloney, 2013: Moisture modes and the eastward propagation of the MJO. *J. Atmos. Sci.*, **70**, 187–192, doi:10.1175/JAS-D-12-0189.1.

——, ——, G. Bellon, and M. F. Dargan, 2008: The role of surface heat fluxes in tropical intraseasonal oscillations. *Nat. Geosci.*, **1**, 653–657, doi:10.1038/ngeo312.

Spencer, M. W., C. Wu, and D. G. Long, 2000: Improved resolution backscatter measurements with the SeaWinds pencil-beam scatterometer. *IEEE Trans. Geosci. Remote Sens.*, **38**, 89–104, doi:10.1109/36.823904.

Sprintall, J., A. L. Gordon, A. Koch-Larrouy, T. Lee, J. T. Potemra, K. Pujiana, and S. E. Wijffels, 2014: The Indonesian seas and their role in the coupled ocean–climate system. *Nat. Geosci.*, **7**, 487–492, doi:10.1038/ngeo2188.

Straub, K. H., 2013: MJO initiation in the real-time multivariate MJO index. *J. Atmos. Sci.*, **26**, 1130–1151, doi:10.1175/JCLI-D-12-00074.1.

Suzuki, T., 2009: Diurnal cycle of deep convection in super clusters embedded in the Madden–Julian oscillation. *J. Geophys. Res.*, **114**, D22102, doi:10.1029/2008JD011303.

Tabata, Y., H. Hashiguchi, M. K. Yamamoto, M. Yamamoto, M. D. Yamanaka, S. Mori, F. Syamsudin, and T. Manik, 2011: Lower tropospheric horizontal wind over Indonesia: A comparison of wind profiler network observations with global reanalyses. *J. Atmos. Sol.-Terr. Phys.*, **73**, 986–995, doi:10.1016/j.jastp.2010.09.016.

Tung, W.-W., D. Giannakis, and A. J. Majda, 2014: Symmetric and antisymmetric convection signals in the Madden–Julian oscillation. Part I: Basic modes in infrared brightness temperature. *J. Atmos. Sci.*, **71**, 3302–3326, doi:10.1175/JAS-D-13-0122.1.

Vitart, F., and F. Molteni, 2010: Simulation of the Madden–Julian oscillation and its teleconnections in the ECMWF forecast system. *Quart. J. Roy. Meteor. Soc.*, **136**, 842–855, doi:10.1002/qj.623.

Waliser, D. E., K. M. Lau, W. Stern, and C. Jones, 2003: Potential predictability of the Madden–Julian oscillation. *Bull. Amer. Meteor. Soc.*, **84**, 33–50, doi:10.1175/BAMS-84-1-33.

Wang, B., 1988: Dynamics of tropical low-frequency waves: An analysis of the moist Kelvin wave. *J. Atmos. Sci.*, **45**, 2051–2065, doi:10.1175/1520-0469(1988)045<2051:DOTLFW>2.0.CO;2.

——, 2005. Theory. *Intraseasonal Variability in the Atmosphere–Ocean Climate System*, W. K.-M. Lau and D. E. Waliser, Eds., Springer, 307–360.

——, and H. Rui, 1990: Dynamics of coupled moist Kelvin–Rossby waves on an equatorial β-plane. *J. Atmos. Sci.*, **47**, 397–413, doi:10.1175/1520-0469(1990)047<0397:DOTCMK>2.0.CO;2.

Weaver, S. J., W. Wang, M. Chen, and A. Kumar, 2011: Representation of MJO variability in the NCEP Climate Forecast System. *J. Climate*, **24**, 4676–4694, doi:10.1175/2011JCLI4188.1.

Wheeler, M. C., and H. H. Hendon, 2004: An all-season real-time multivariate MJO index: Development of an index for monitoring and prediction. *Mon. Wea. Rev.*, **132**, 1917–1932, doi:10.1175/1520-0493(2004)132<1917:AARMMI>2.0.CO;2.

Wu, C. H., and H. H. Hsu, 2009: Topographic influence on the MJO in the Maritime Continent. *J. Climate*, **22**, 5433–5448, doi:10.1175/2009JCLI2825.1.

Xie, P., and P. A. Arkin, 1997: Global precipitation: A 17-year monthly analysis based on gauge observations, satellite estimates, and numerical model outputs. *Bull. Amer. Meteor. Soc.*, **78**, 2539, doi:10.1175/1520-0477(1997)078<2539:GPAYMA>2.0.CO;2.

Xu, W., and S. A. Rutledge, 2014: Convective characteristics of the Madden–Julian oscillation over the central Indian Ocean observed by shipborne radar during DYNAMO. *J. Atmos. Sci.*, **71**, 2859–2877, doi:10.1175/JAS-D-13-0372.1.

Yanai, M., S. Esbensen, and J. H. Chu, 1973: Determination of bulk properties of tropical cloud clusters from large-scale heat and moisture budgets. *J. Atmos. Sci.*, **30**, 611–627, doi:10.1175/1520-0469(1973)030<0611:DOBPOT>2.0.CO;2.

Zhang, C., 2013: Madden–Julian oscillation: Bridging weather and climate. *Bull. Amer. Meteor. Soc.*, **94**, 1849–1870, doi:10.1175/BAMS-D-12-00026.1.

——, and M. Dong, 2004: Seasonality in the Madden–Julian oscillation. *J. Climate*, **17**, 3169–3180, doi:10.1175/1520-0442(2004)017<3169:SITMO>2.0.CO;2.

——, and J. Ling, 2012: Potential vorticity of the Madden–Julian oscillation. *J. Atmos. Sci.*, **69**, 65–78, doi:10.1175/JAS-D-11-081.1.

Zhou, L., and Y. Wang, 2006: Tropical Rainfall Measuring Mission observation and regional model study of precipitation diurnal cycle in the New Guinean region. *J. Geophys. Res.*, **111**, 1984–2012, doi:10.1029/2006JD007243.

Unauthenticated | Downloaded 12/28/22 07:27 PM UTC